Published OnlineFirst October 31, 2013; DOI: 10.1158/0008-5472.CAN-13-0436

CD4 T Lymphocyte Enrichment kit (BD Pharmingen). Then, cells were stimulated with PMA/Io for 9 hours, RNA was isolated, and reverse transcription was performed as described earlier. cDNA products were analyzed by real-time PCR using the Taqman Universal PCR Master Mix (PE Applied Biosystems) or FastStart Universal SYBR Green Master (Roche) and Applied Biosystems StepOnePlus Real-Time PCR System according to the manufacturer's instructions. Specific primers and Taqman probes for the *Bim* gene, *FasL* gene, and *GAPDH* internal control gene were purchased from Applied Biosystems. Primer sequences for the *HBZ* gene and *GAPDH* gene used for the evaluation of the knockdown efficiency in MT-1 cells have been described previously (11, 23). Primer sequences for the *HBZ* gene used for another experiment to evaluate the HBZ expression in Jurkat-HBZ, MT-1, TL-Om1, and ED cells were 5′-ATGGCGGCCTCAGGGCTGTT-3′ and 5′-GCGGCTTTCCTCTTCTAAGG-3′. Primer sequences for the *FoxO3a* gene used were 5′-ACAAACGGCTCACTCTGTCCCAG-3′ and 5′-AGCTCTTGCCAGTTCCCTCATTCTG-3′. All amplifications were conducted in triplicates. The relative quantification was calculated according to the method described in Applied Biosystems ABI prism 7700 SDS User Bulletin #2.

Chromatin immunoprecipitation analysis

Chromatin immunoprecipitation (ChIP) assay was performed according to the protocol recommended by Millipore. Cells were fixed with 1% formaldehyde for 10 minutes at room temperature, washed twice with ice-cold PBS, treated with SDS-lysis buffer (1% SDS, 50 mmol/L EDTA, and 200 mmol/L Tris-HCl) for 10 minutes on ice and then sonicated. Thereafter, the DNA/protein complexes were immunoprecipitated with antibodies specific for acetylated-Histone H3, acetylated-Histone H4, dimethylated-Histone H3 (Lys4), RNA polymerase II clone CTD4H8 (Millipore), trimethylated-Histone H3 (Lys27), anti-trimethyl-Histone H3 (Lys9) antibodies (Cell Signaling Technology), or normal rabbit IgG (Santa Cruz Biotechnology) overnight at 4°C. Immune complexes were collected with salmon sperm DNA-protein A and G Sepharose slurry, washed, and eluted with freshly prepared elution buffer (1% SDS, 100 mmol/L $NaHCO_3$). Protein-DNA complexes were de-cross-linked at 65°C for 4 hours. DNA was purified and subjected to real-time PCR for quantification of the target fragments. Sequences for the primer set are described previously (24, 25). For the evaluation of binding of FoxO3a to the FOXO-binding sites, 293T cells were transfected with 5 μg of 6xDBE-Luc construct, 5 μg of FoxO3aAAA expression plasmid together with or without 5 μg of HBZ plasmid using TransIT in 10-cm dishes. Anti-FLAG (Sigma) antibody was used for the immunoprecipitation. Primers used were 5′-AGTGCAGGTGCCAGAACATT-3′ and 5′-GCCTTATGCAGTTGCTCTCC-3′, which were constructed inside of the pGL3-basic vector. For the evaluation of the DNA-binding capacity of FoxO3a with or without HBZ, expression vectors for the HA-tagged FoxO3a and Flag-tagged HBZ were transiently cotransfected into 293T cells using the TransIT reagent. Twenty-four hours after the transfection, cells were collected and chromatin immunoprecipitation assay was performed as described earlier. For the immunoprecipitation, anti-HA (Sigma) antibody was used. Primers used for *Bim* gene promoter were 5′-CCACCACTTGATTCTTGCAG-3′ and 5′-TCCAGCGCTAGTCTTCCTTC-3′, which were constructed to contain the FOXO-binding sequence located in intron1. Primers used for *FasL* gene promoter were 5′-ACGATAGCACCACTGCACTCC-3′ and 5′-GGCTGCAAACCAGTGGAAC-3′, which were also constructed to contain the three FOXO-binding sequences.

Individual PCRs were carried out in triplicate to control for PCR variation and mean C_t values were collected. Fold difference of the antibody-bound fraction (IP) versus a fixed amount of input (In) was calculated as

$$\mathrm{IP/In} = 2^{-\Delta\Delta C_t} = 2^{-(C_t(\mathrm{IP}) - C_t(\mathrm{In}))}$$

Then, the fold difference value for a target antibody (t) was subtracted by the nonspecific value derived from mouse or rabbit IgG (t_0):

$$(\mathrm{IP/In})^t - (\mathrm{IP/In})^{t_0}$$

Bisulfite genomic sequencing

Sodium bisulfite treatment of genomic DNA was performed as described previously (26). DNA regions were amplified using bisulfite-treated genomic DNA by nested PCR. To amplify promoter region (promoter 1) of *Bim*, primers used in the first PCR were 5′-TTTAGAGGGAGGAGAGTTTAAAG-3′ and 5′-CCCTACAACCCAACTCTAACTA-3′. Primers for the second PCR were 5′-AGGGTATAGTGAGAGCGTAGG-3′ and 5′-CAACTCTAACTAACGACCCC-3′. For promoter, two primers used in the first PCR were 5′-GTGTGATTGTTTTTTGAGGG-3′ and 5′-AAAATACCCCCAAACAAAATAC-3′. Primers for the second PCR were 5′-GCGGATTTAGTTGTAGATTTTG-3′ and 5′-ACTCTTTACCCAAAACAAACTTC-3′. PCR products were purified, cloned into pGEM-T Easy vector (Promega), and sequenced using the ABI PRISM 3130 Genetic Analyzer. For CpG methylation analysis, Web-based bisulfite sequencing analysis tool called QUMA (quantification tool for methylation analysis) was used (27).

Coimmunoprecipitation assay, analysis of the p-FoxO3a localization, and immunoblotting

Expression vectors for the relevant genes were transiently cotransfected into 293T cells using the TransIT reagent. Forty-eight hours later, cells were collected and coimmunoprecipitation assays were performed as described previously (28). For the analysis of the p-FoxO3a localization, nuclear and cytoplasmic proteins were extracted using Nuclear Complex Co-IP Kit (Active Motif). The proteins were subjected to SDS-PAGE analysis followed by immunoblotting with various antibodies. Antibodies used were anti-p-FoxO3a, anti-α-tubulin (Sigma), anti-FLAG, anti-HA (Sigma), and anti-His (Marine Biological Laboratory).

Lentiviral vector construction and transfection of the recombinant lentivirus

Lentiviral vector expressing shRNA against HBZ was constructed and recombinant lentivirus was infected as described previously (11). When more than 90% of cells expressed

Published OnlineFirst October 31, 2013; DOI: 10.1158/0008-5472.CAN-13-0436

enhanced green fluorescent protein (EGFP), the *HBZ* and *Bim* gene expressions were analyzed by real-time PCR.

Results

The *Bim* gene transcription is suppressed in HBZ-expressing Jurkat and CCRF-CEM cells

To determine the effects of HBZ on gene expression, we first performed microarray analysis. Jurkat cells with or without expression of spliced form of HBZ (Jurkat-HBZ and Jurkat-control, respectively) were stimulated with PMA and Io for 9 hours. Gene expression profiles were then analyzed by DNA microarray. Table 1 shows the apoptosis-associated genes that were downregulated or upregulated in stimulated Jurkat-HBZ cells. Transcription of the *Bim* gene was prominently downregulated in HBZ-expressing Jurkat cells. To confirm the effect of HBZ on the *Bim* gene expression, we evaluated *Bim* mRNA levels in Jurkat-control and Jurkat-HBZ cells with or without PMA/Io stimulation using real-time PCR. As reported in the previous studies showing that treatment by PMA/Io or other stimulators induced *Bim* expression (29, 30), the *Bim* mRNA level of stimulated Jurkat-control cells was three-times higher than that of unstimulated cells, but that of Jurkat-HBZ cells did not change after stimulation (Fig. 1A). Similarly, increased *Bim* transcription by stimulation was also inhibited by HBZ in CCRF-CEM cells (Fig. 1A).

HBZ inhibits apoptosis

It has been reported that Bim plays an important role in activation-induced cell death and T-cell homeostasis (31). Because the earlier data demonstrated that HBZ inhibits stimulation-induced *Bim* expression, we next investigated whether HBZ inhibits apoptosis in response to PMA/Io stimulation. To test this, Jurkat-control and Jurkat-HBZ were each incubated with or without PMA/Io for 9 hours, and then apoptosis was measured using Annexin V. The percentages of apoptotic cells in Jurkat-control and Jurkat-HBZ were 40.2% and 15% respectively, indicating that HBZ suppressed activation-induced apoptosis (Fig. 1B). We also treated cells with doxorubicin and found that HBZ slightly inhibited doxorubicin-induced apoptosis (Supplementary Fig. S1). Fas-mediated apoptotic pathway might be involved in antiapoptotic effect by HBZ. To assess the effect of Fas-mediated signaling on the activation-induced apoptosis, cells were also treated with or without Fas-blocking antibody (0.5 μg/mL) 30 minutes before the PMA/Io stimulation. The percentage of apoptotic cells without Fas-blocking antibody in Jurkat-control and Jurkat-HBZ were 36.9% and 22.4%, respectively. When cells were treated with Fas-blocking antibody, the percentage of apoptotic cells reduced and those were 24% and 13.2% in Jurkat-control and Jurkat-HBZ, respectively (Fig. 1C). Thus, Fas-blocking antibody partially inhibited apoptosis in Jurkat-HBZ, which indicates that Fas-mediated signals are also implicated in activation-induced cell death. Indeed, we found that the transcription level of *FasL* was suppressed in stimulated Jurkat-HBZ and CEM-HBZ cells compared with Jurkat-control and CEM-control cells (Fig. 1D), suggesting that downregulation of FasL by HBZ was also associated with inhibition of apoptosis.

Table 1. Apoptosis-associated genes that are upregulated or downregulated by HBZ

Gene	Fold change	Gene ontology
API5	2.18	Antiapoptosis
BCL2L11 (Bim)	−9.93	Induction of apoptosis
CARD11	2.87	Regulation of apoptosis
CASP1	2.97	Apoptosis
CD28	4.60	Positive regulation of antiapoptosis
COP1	9.41	Regulation of apoptosis
DEDD2	2.01	Induction of apoptosis via death domain receptors
DYRK2	2.16	Induction of apoptosis
GZMB	−5.90	Apoptosis
HIPK2	2.19	Induction of apoptosis by intracellular signals
NLRP1	3.08	Induction of apoptosis
PI3KR2	−2.68	Negative regulation of antiapoptosis
PLEKHF1	2.99	Induction of apoptosis
PRDX2	−2.10	Antiapoptosis
PRF1	3.95	Virus-infected cell apoptosis
RFFL	2.20	Apoptosis
SPHK1	−4.26	Antiapoptosis
TNFRSF9	−2.61	Induction of apoptosis
TP53INP1	2.32	Apoptosis
VEGFA	−6.96	Negative regulation of apoptosis

NOTE: The table shows a list of apoptosis-associated genes that were downregulated or upregulated (by more than 2-fold) in stimulated Jurkat-HBZ cells identified by microarray analysis.

Published OnlineFirst October 31, 2013; DOI: 10.1158/0008-5472.CAN-13-0436

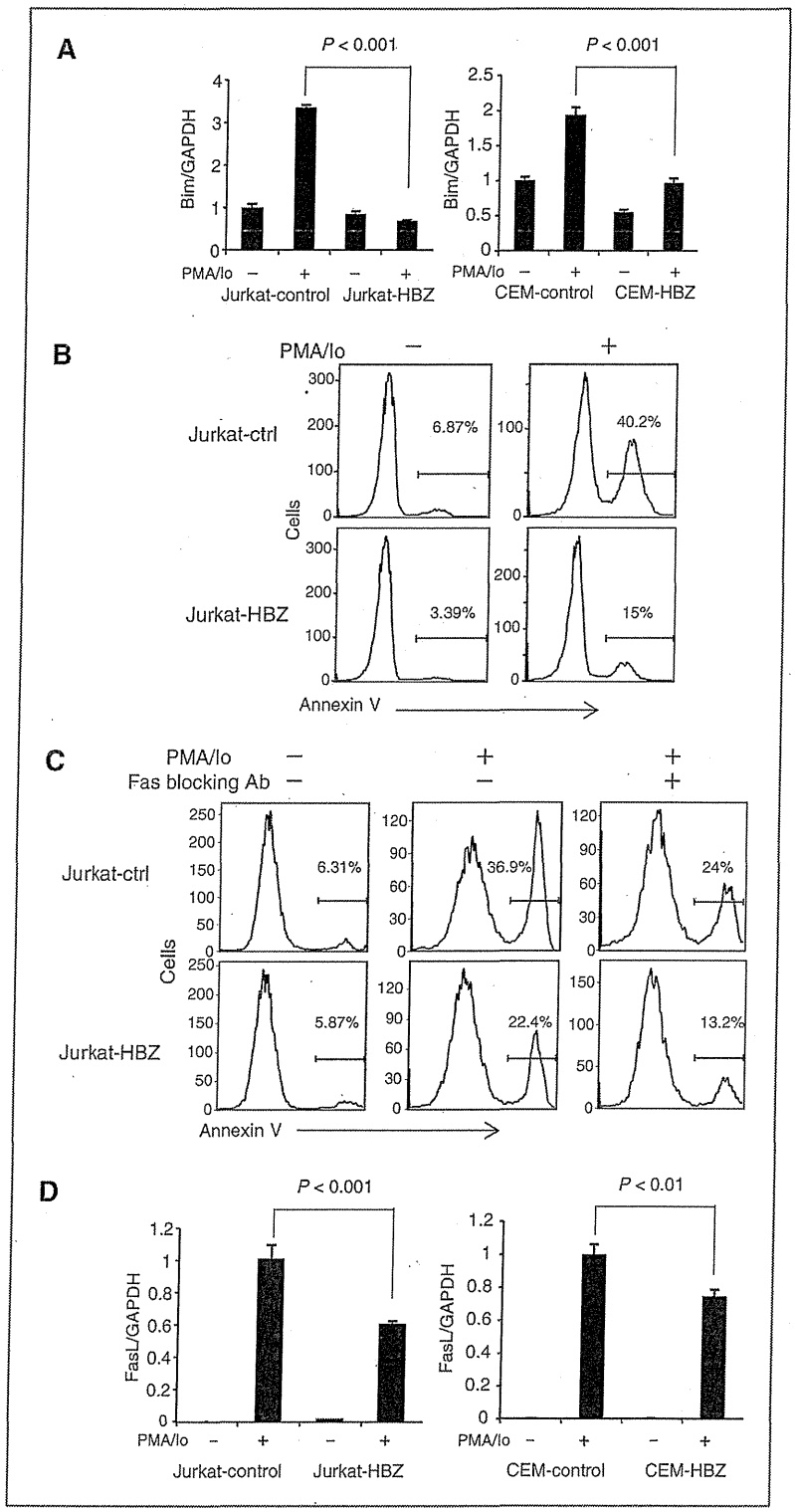

Figure 1. HBZ suppresses the transcription of the *Bim* and *FasL* genes and consequently stimulation-induced apoptosis. A, comparison of the *Bim* mRNA expression in the Jurkat-control, Jurkat-HBZ, CEM-control, and CEM-HBZ cells with or without PMA/Io stimulation by real-time PCR. B, Jurkat-control and Jurkat-HBZ were stimulated with PMA/Io for 9 hours and stained with Annexin V. Percentage of apoptotic cells was determined by flow cytometry. C, Jurkat-control and Jurkat-HBZ were treated with Fas-blocking antibody for 30 minutes and then stimulated with PMA/Io for 9 hours. Percentages of apoptotic cells were monitored by flow cytometry. D, comparison of the *FasL* mRNA transcription in the Jurkat-control, Jurkat-HBZ, CEM-control, and CEM-HBZ cells with or without PMA/Io stimulation by real-time PCR. Error bars, standard deviation. Statistical differences are calculated by Student *t* test. GAPDH, glyceraldehyde-3-phosphate dehydrogenase.

Published OnlineFirst October 31, 2013; DOI: 10.1158/0008-5472.CAN-13-0436

HBZ suppresses *Bim* expression through attenuation of FoxO3a

We analyzed how HBZ suppresses the expression of *Bim* and *FasL*. It has been reported that a forkhead factor, FoxO3a, and p73 are important for the transcription of *Bim* and *FasL* (32, 33). FoxO3a and other FOXO family members are phosphorylated by protein kinases such as Akt or SGK on highly conserved serine and threonine residues (especially Thr32, Ser253, and Ser315 in FoxO3a), resulting in impaired DNA-binding activity and increased binding to the chaperone protein, 14-3-3 (20, 34, 35). Newly formed 14-3-3-FOXO complexes are then exported from the nucleus, thereby inhibiting FOXO-dependent transcription of key target genes such as *Bim*, *FasL*, and *TRAIL* (36).

First, we investigated whether FoxO3a is implicated for the activation induced cell death. As shown in Supplementary Fig. S2, the knockdown of FoxO3a resulted in the decreased apoptotic rate in Jurkat-control cells ($P < 0.05$). Furthermore, inhibition of Foxo3a did not influence activation-induced cell death in Jurkat-HBZ cells, suggesting the inhibitory effect of HBZ on Foxo3a function. To investigate whether HBZ affects FoxO3a function, Jurkat cells were transiently transfected with a plasmid expressing FoxO3aAAA, the constitutive active mutant of FoxO3a, which is no longer phosphorylated by Akt and is localized in the nucleus. The FoxO3aAAA was expressed together with hrGFP using an internal ribosome entry site (IRES; FoxO3aAAA-IREShrGFP). Jurkat cells were transiently transfected with full-length HBZ or its mutants. HBZ has three domains, an activation domain (AD), a central domain (CD), and a basic leucine zipper domain (bZIP; ref. 12). In this study, the deletion mutants (HBZ-ΔAD, HBZ-ΔbZIP, and HBZ-ΔCD) were used. The percentage of FoxO3aAAA induced apoptotic cells in the absence of HBZ was 69.6% while it was suppressed by HBZ (40.6%; $P < 0.001$; Fig. 2A). We also found that an HBZ mutant without activation domain lacks the activity to inhibit FoxO3aAAA-induced apoptosis (Fig. 2A), indicating the significance of activation domain in suppression of FoxO3a-mediated apoptosis. It has been reported that LXXLL motif in FoxO3a binds to its coactivator CBP/p300 (37). Similarly, HBZ has LXXLL-like motifs located in the NH_2-terminal region, which bind to KIX domain of CBP/p300 (38). We speculated that the LXXLL-like motifs of HBZ might affect FoxO3aAAA function through KIX domain of CBP/p300. An HBZ mutant, which has substitutions in 27th and 28th residues (LL to AA) of LXXLL-like motif, lack the activity to suppress FoxO3aAAA-mediated apoptosis (Fig. 2B), indicating that LXXLL-like motif of HBZ is critical for suppression of FoxO3a-mediated apoptosis.

Next, we analyzed the effect of HBZ on a FoxO3a responsive reporter. As shown in Fig. 2C, HBZ suppressed FoxO3a-mediated transcriptional activity ($P < 0.01$). To check whether HBZ inhibits DNA binding of FoxO3a, 293T cells were transiently transfected with FoxO3aAAA and FoxO3a reporter, 6xDBE-Luc, together with or without HBZ. The interaction of FoxO3aAAA to FOXO-binding sites was analyzed by ChIP assay. As shown in Figure 2D, the interaction of FoxO3aAAA to the FOXO-binding sites was interfered by HBZ, suggesting that HBZ inhibits FoxO3a-mediated apoptosis through suppression of the DNA binding of FoxO3a. To clarify the mechanism of HBZ-mediated FoxO3a inhibition, we examined interaction between HBZ and FoxO3a by the immunoprecipitation assay. It showed that HBZ interacted with FoxO3a (Fig. 2E and F). Experiments with FoxO3a deletion mutant revealed that HBZ interacted with the forkhead domain of FoxO3a (Fig. 2E). Analysis using HBZ deletion mutants showed that the central domain of HBZ interacted with FoxO3a (Fig. 2F).

HBZ inhibits nuclear export of phosphorylated form of FoxO3a

Next, we investigated the effect of HBZ on FoxO3a localization by confocal microscopy. We cotransfected 293FT cells with a plasmid expressing human wild-type FoxO3a (FoxO3aWT) protein and an HBZ-expressing plasmid. Consistent with previous reports, FoxO3a remained mainly in cytoplasm when cells were cotransfected with empty vector (Fig. 3A; refs. 20, 34). However, when it was expressed along with HBZ, FoxO3a was localized in both nucleus and cytoplasm (Fig. 3A). To determine whether mislocalized FoxO3a is phosphorylated (pFoxO3a) or not, we used anti-pFoxO3a antibody. Figure 3B and C demonstrated that nuclear-localized FoxO3a was phosphorylated in HBZ-expressing cells. Thereafter, we analyzed the localization of endogenous FoxO3a in HeLa and an ATL cell line, MT-1. Although pFoxO3a was localized widely both in cytoplasm and nucleus in HeLa cells, most pFoxO3a was localized in the nucleus in MT-1 (Fig. 3D), suggesting that endogenous HBZ inhibits the extranuclear translocation of pFoxO3a in this cell line. From the study of crystal structure of the human FoxO3a-DBD/DNA complex, it has been reported that phosphorylation at Ser253 causes a decrease on the DNA-binding ability (39). Abnormal localization of phosphorylated FoxO3a by HBZ might interfere the function of unphosphorylated FoxO3a in the nucleus. The abnormal localization of pFoxO3a prompted us to investigate whether HBZ bound to 14-3-3 along with FoxO3a, as 14-3-3 is a chaperon protein involved in nuclear–cytoplasm shuttling of FOXO family. As shown in Figure 3E, HBZ, FoxO3a, and 14-3-3 form a ternary complex. However, the binding of FoxO3a and 14-3-3 was not affected by HBZ (result of IP with anti-FLAG antibody and detected with anti-HA antibody).

As another possible mechanism for downregulation of *Bim* and *FasL*, we compared the transcription level of *p73* in Jurkat cells with and without HBZ expression. Activation of HBZ-expressing cells reduced transcription of *p73*, but the expression level of *p73* was variable among ATL cell lines (Supplementary Fig. S3A and S3B). We conclude that p73 is not responsible for suppression of *Bim* expression in ATL cells.

Bim expression is suppressed in both ATL cell lines and ATL cases

HBZ has been shown to suppress Bim expression through two different mechanisms as revealed in this study. To analyze Bim expression in ATL cells, we studied *Bim* mRNA levels in non-ATL cell lines and ATL cell lines with or without PMA/Io stimulation, and found that the *Bim* gene transcript was upregulated in Jurkat and CCRF-CEM cells, but not in SupT1 after activation. However, *Bim* transcripts were not increased

Published OnlineFirst October 31, 2013; DOI: 10.1158/0008-5472.CAN-13-0436

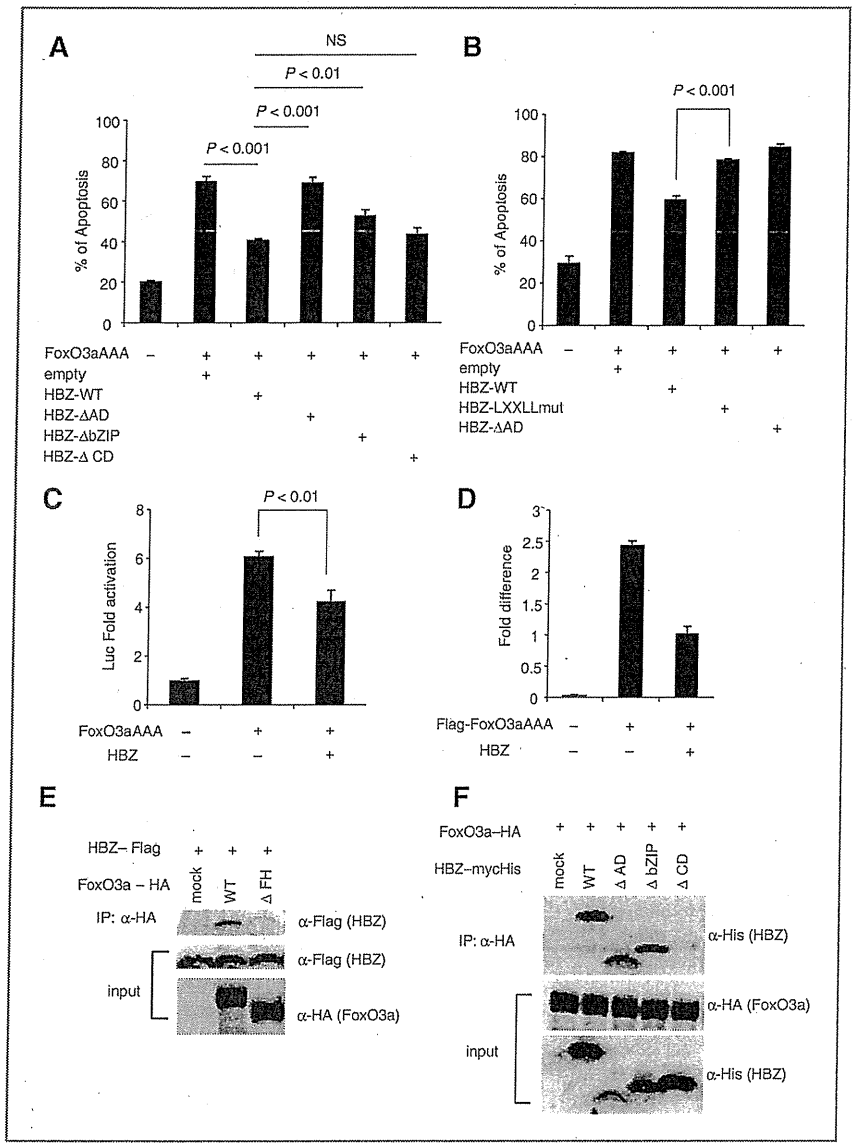

Figure 2. HBZ attenuates function of Foxo3a by physical interaction. A, Jurkat cells were transfected with FoxO3aAAA-expressing vector, a constitutively active form, by using Neon with or without HBZ or its mutants. Twenty-four hours after transfection, cells were stained with Annexin V and analyzed by flow cytometry ($n = 3$). B, Jurkat cells were transfected with FoxO3aAAA-expressing vector together with HBZ or its mutants by using Neon. Cells were stained with Annexin V and analyzed by flow cytometry ($n = 3$). Data are representative of three independent experiments. C, reporter construct containing the 6xDBE and FoxO3aAAA-expressing vector was transiently transfected with or without HBZ into Jurkat cells in the presence of Z-VAD-FMK and luciferase activities were measured. D, 293T cells were transfected with 6xDBE-Luc construct and Flag-tagged FoxO3aAAA expression vector together with or without HBZ expression vector. Cells were immunoprecipitated with anti-FLAG antibody and quantified by real-time PCR. Three independent ChIP experiments were done and representative data are shown. Error bars, experimental variation. E and F, the expression vectors of the indicated proteins were cotransfected into 293T cells, and their interactions were analyzed by immunoprecipitation assay. Data are representative of three independent experiments. Statistical differences are calculated by Student *t* test.

in all stimulated ATL cell lines (Fig. 4A). The *Bim* gene transcript was also downregulated in primary ATL cells (Fig. 4B) compared with resting peripheral blood mononuclear cells (PBMC) and phytohemagglutinin (PHA)-stimulated T cells. We also stimulated primary ATL cells and normal $CD4^+$ T cells with PMA/Io. The *Bim* gene transcription was quite low in primary ATL sample compared with normal $CD4^+$ T cells even though the cells were stimulated with PMA/Io (Fig. 4C). To confirm HBZ expression in representative ATL cell lines, we quantified the level of the *HBZ* mRNA transcription in Jurkat-HBZ, CEM-HBZ, MT-1, ED, and TL-Om1 by real-time PCR and confirmed that HBZ is expressed in these ATL cell lines (Supplementary Fig. S4). Microarray data, obtained from Gene Expression Omnibus (GEO), show that both *Bim* and *FasL* transcription levels are lower in ATL cases than healthy donors (accession number: GSE33615; Supplementary Fig. S5), supporting our data that *Bim* expression was suppressed in ATL cells.

Bim expression is silenced by epigenetic mechanisms

Because the *Bim* gene transcription was severely suppressed in ATL cells, we investigated the epigenetic status (DNA methylation and histone modification) of the promoter region of the *Bim* gene in ATL cells. A previous study showed that the 0.8 kb region immediately upstream of exon 1 contains the important elements for the control of *Bim* expression

Published OnlineFirst October 31, 2013; DOI: 10.1158/0008-5472.CAN-13-0436

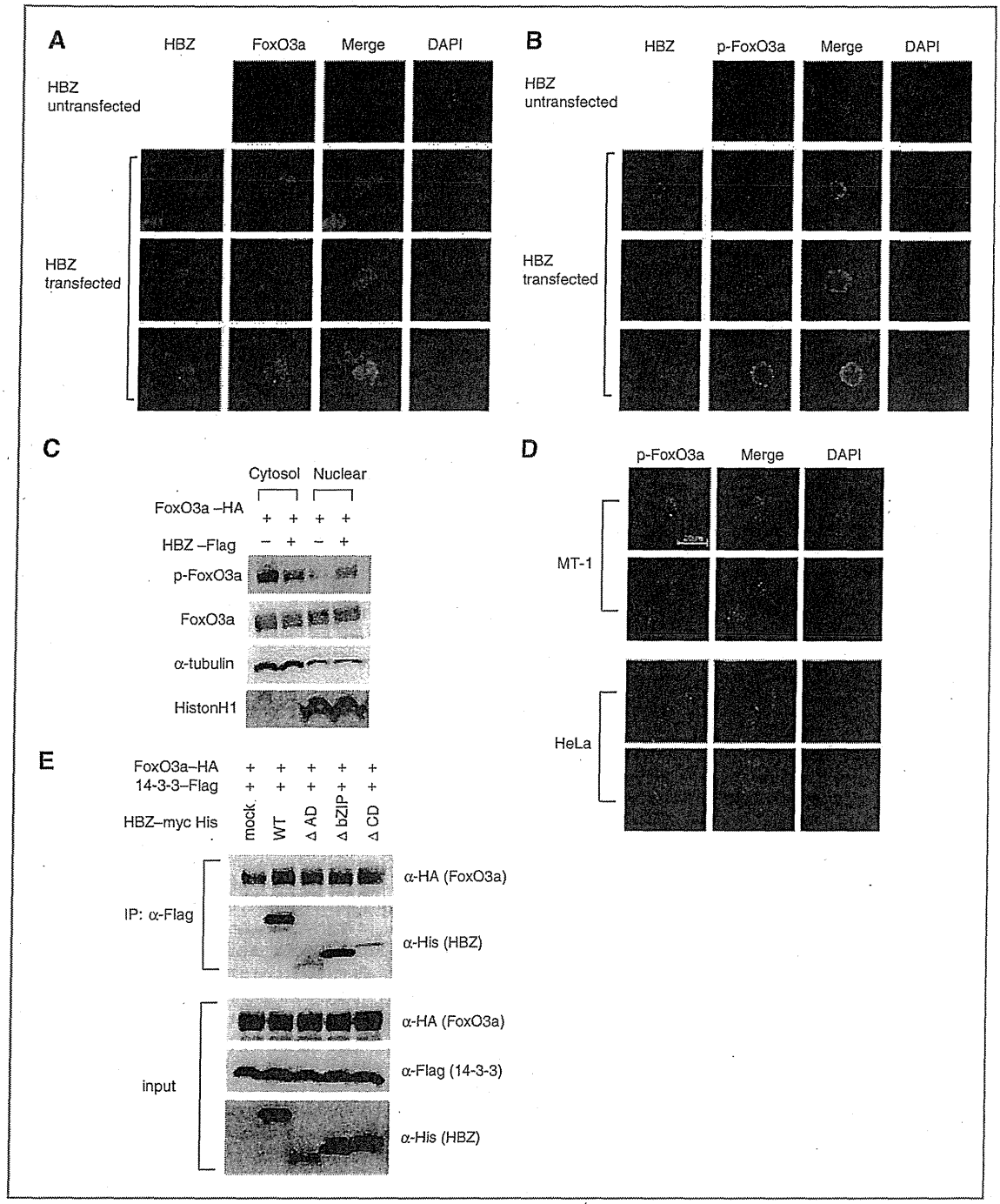

Figure 3. HBZ interferes with normal localization of FoxO3a by forming a ternary complex with FoxO3a and 14-3-3. 293FT cells were transfected with FoxO3aWT-Flag together with or without mycHis-HBZ. A and B, FoxO3a was detected using anti-FLAG-biotin and secondary Streptavidin-Alexa 488 (A), and p-FoxO3a was detected using anti-p-FoxO3a (ser253) and secondary anti-rabbit IgG-Alexa 488 antibody (B). DAPI was used to counterstain the nucleus. C, 293FT cells were transfected with HA-tagged FoxO3aWT together with or without Flag-tagged HBZ. Cytoplasmatic and nuclear fractions were extracted and p-FoxO3a was detected by Western-blotting. D, endogenous localizations of p-FoxO3a (ser253) in HeLa and MT-1 cells were examined using anti-p-FoxO3a. E, the interactions among HBZ, FoxO3a, and 14-3-3 were analyzed by immunoprecipitation.

Published OnlineFirst October 31, 2013; DOI: 10.1158/0008-5472.CAN-13-0436

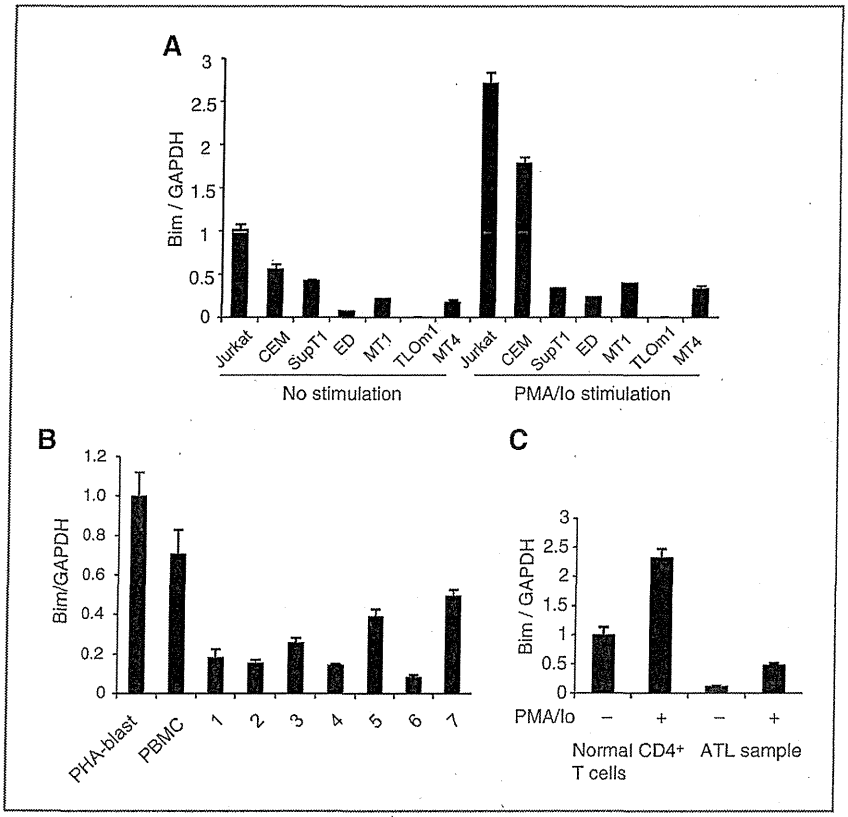

Figure 4. Bim expression is also suppressed in ATL cell lines and ATL cases. Comparison of the *Bim* mRNA expression in non-ATL cell lines and ATL cell lines with or without PMA/Io stimulation (A) and in PBMCs and PHA-blasts from healthy donor samples and fresh ATL samples (B) by real-time PCR. C, comparison of the *Bim* mRNA expression in healthy donor sample and ATL fresh sample with or without PMA/Io stimulation.

(promoter 1). The *Bim* promoter does not contain a TATA or CAAT box and has the characteristics of a "TATA-less" promoter (40). In addition, the alternative promoter has been reported to exist in intron 1 (promoter 2; refs. 41, 42). These two promoter regions are highly GC-rich and contain the binding sites for several transcription factors, including FoxO3a. To determine whether CpG sites in these *Bim* gene promoter regions are methylated in ATL cell lines, their methylation status was analyzed by bisulfite-mediated methylcytosine mapping (Supplementary Fig. S6A and S6B). The promoter 1 of *Bim* was hypermethylated in two ATL cell lines (ED and TL-Om1) and ATL case 1, whereas this region was not so methylated in MT-1 cells and two ATL cases. On the other hand, the promoter 2 was heavily methylated in two ATL cell lines (TL-Om1 and MT-1) and ATL case 1 and partially methylated in Jurkat cells (Supplementary Fig. S6B). These results suggest that in some cases, heavily methylated CpG sites of promoter 1 and 2 are associated with silencing of *Bim* transcription but these methylations can not account for suppressed *Bim* expression in all ATL cell lines and ATL cases.

Therefore, we next focused on the histone modification in the promoter region of *Bim*. It is well known that deacetylation of the histones are also common features of cancer, which results in transcriptional silencing of tumor suppressor genes (43). First, we analyzed the histone H3 and H4 acetylation and H3K4 trimethylation, which are all permissive marks (44), in promoter 1 of Jurkat, MT-1, and TL-Om1 cells. Contrary to our speculation, neither H3, H4 acetylation, nor H3K4 trimethylation differed between MT-1 and Jurkat cells (Supplementary Fig. S7). We next analyzed the histone modification status in promoter 2. As shown in Figure 5A, MT-1 and TL-Om1 cells exhibited decreased level of histone H3 acetylation and H3K4 trimethylation but not histone H4 acetylation. Because methylation of DNA is often preceded by dimethylation of H3K9 or trimethylation of H3K27 (both repressive marks) in oncogenesis (44), we asked whether there were differences in these epigenetic chromatin marks on the *Bim* gene promoter in ATL cell lines. TL-Om1 cells exhibited upregulated level of H3K9 dimethylation and H3K27 trimethylation compared with Jurkat cells (Fig. 5B and C), whereas MT-1 exhibited a little upregulated level of H3K27 trimethylation (Fig. 5C) in the promoter 2. These data suggest that histone modifications of promoter 2 are critical for the suppressed *Bim* gene transcription. We also performed ChIP analysis using anti-RNA polymerase II antibody (Fig. 5D) and revealed that Pol II binding was decreased in MT-1 and TL-Om1 cells, confirming suppressed transcription of the *Bim* gene. To further investigate the mechanisms involved in FoxO3a-mediated *Bim* gene transcription in the promoter 2, we transfected HA-tagged FoxO3a expression vector together with or without a HBZ expression vector into 293T cells and immunoprecipitated with anti-HA antibody. Then, the DNA-binding capacity of FoxO3a was

Published OnlineFirst October 31, 2013; DOI: 10.1158/0008-5472.CAN-13-0436

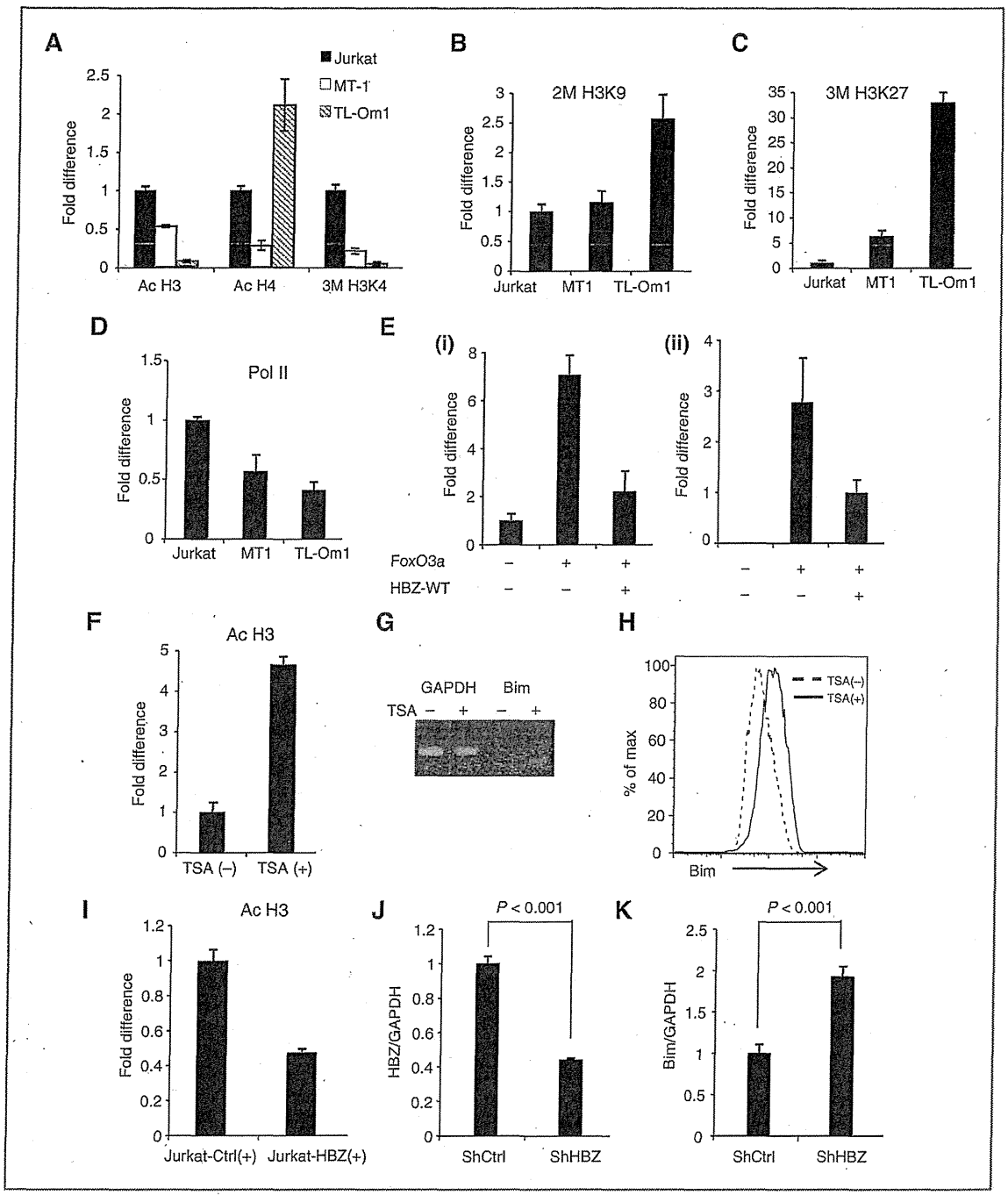

Figure 5. Epigenetic status of the promoter regions of the *Bim* gene. A–C, fold difference of acetylated histone H3, acetylated histone H4, trimethylated H3K4, dimethylated H3K9, or trimethylated H3K27; the data from Jurkat cells were arbitrarily set as 1.0. D, quantitative ChIP assay using RNA polymerase II (Pol II) antibody in Jurkat, MT-1, and TL-Om1 cells. E, 293T cells were transfected with HA-tagged FoxO3a expression vector together with or without HBZ expression vector. Cells were immunoprecipitated with anti-HA antibody and DNA-binding ability at promoter 2 was quantified by real-time PCR. F, fold difference of acetylated histone H3 in MT-1 cells, which were treated with or without 0.4 mmol/L TSA for 15 hours. The data from MT-1 cells without TSA treatment were arbitrarily set as 1.0. G and H, MT-1 cells were treated with 0.4 mmol/L TSA for 15 hours and *Bim* expression level was analyzed by quantitative real-time PCR and flow cytometry. I, fold difference of acetylated histone H3 in the Bim promoter in the Jurkat-control and Jurkat-HBZ cells 9 hours after the stimulation with PMA/Io. J, HBZ transcript in shRNA transfectant of MT-1 was quantified by real-time PCR. K, comparison of the *Bim* mRNA expression in control MT-1 cells and HBZ-KD MT-1 cells. Error bars, experimental variation. The data shown are representative of two or three independent experiments. Statistical differences are calculated by Student *t* test. GAPDH, glyceraldehyde-3-phosphate dehydrogenase.

Published OnlineFirst October 31, 2013; DOI: 10.1158/0008-5472.CAN-13-0436

quantified by real-time PCR. Figure 5E shows that HBZ attenuated the DNA-binding capacity of FoxO3a in the promoter 2 of *Bim* (i) and *FasL* promoter (ii), suggesting that the suppressed binding of FoxO3a to the promoter regions leads to inhibition of the *Bim* and *FasL* genes transcription by HBZ.

Next, we treated MT-1 cells with trichostatin A (TSA), a cell-permeable chemical inhibitor of class I/II histone deacetylases (HDAC). Treatment of TSA resulted in a clear upregulation of acetylation of histone H3 (Fig. 5F) followed by Bim expression both at the mRNA (Fig. 5G) and protein levels (Fig. 5H), indicating that histone modification is associated with suppressed *Bim* transcription in MT-1. We also performed ChIP assay using Jurkat-control and Jurkat-HBZ cells, which were stimulated with PMA and ionomycin for 9 hours, and found that acetylation of histone H3 decreased in Jurkat-HBZ cells (Fig. 5I), suggesting that HBZ is implicated in histone deacetylation in T cells. To verify whether HBZ inhibits transcription of the *Bim* gene, we suppressed the *HBZ* gene transcription by shRNA as reported previously (11). Efficiencies of lentivirus vector transduction, which were determined by EGFP expression, were 90.5% and 90.3% for control MT-1 cells and HBZ-knockdown MT-1 cells, respectively. Suppressed HBZ expression led to increase the *Bim* gene transcription (Fig. 5J and K), indicating that HBZ expression is linked to suppression of *Bim* expression in ATL cells.

Discussion

Human immunodeficiency virus type 1 (HIV-1) replicates vigorously and the generated virus infects target cells *in vivo*. Unlike HIV-1, HTLV-1 induces proliferation to increase the number of infected cells, as this virus is transmitted primarily by cell-to-cell contact (5). Therefore, HTLV-1–encoded proteins promote proliferation of infected cells and inhibit their apoptosis, resulting in an increased number of infected cells *in vivo* (2). In this study, we show that HBZ inhibits both the intrinsic and extrinsic apoptotic pathways via targeting FoxO3a, which leads to suppressed transcriptions of *Bim* and *FasL*. We demonstrated two mechanisms for perturbation of FoxO3a by HBZ: interaction of HBZ with FoxO3a and interference of nuclear export of phosphorylated FoxO3a. HBZ suppresses DNA-binding ability of active form of FoxO3a through interaction between central domain of HBZ and forkhead domain of FoxO3a. In addition, LXXLL-like motif of HBZ is implicated in inhibition of FoxO3a-mediated apoptosis, suggesting that HBZ interferes in interaction of CBP/p300 and FoxO3a. Furthermore, HBZ retains inactive form of FoxO3a in the nucleus through interaction with 14-3-3, leading to transcriptional repression of the target genes. Interestingly, accumulation of phosphorylated form of FoxO3a in the nucleus has been observed in HIV Vpr-expressing cells, which might be implicated in HIV-mediated resistance against insulin (28). Thus, FoxO3a is a target of both human retroviruses.

In this study, we showed that central domain of HBZ interacts with FoxO3a while LXXLL-like motif in activation domain of HBZ is responsible for suppressed apoptosis. LXXLL-like motif of HBZ has been reported to interact with KIX domain of p300 (38). The central domain of HBZ interacts with the forkhead domain of FoxO3a, which binds to the target sequence (35). This is the mechanism how HBZ inhibits DNA binding of FoxO3a. However, inhibitory effect of HBZ on apoptosis largely depends on LXXLL-like motif of activation domain (Fig. 2A and B). FoxO3a is also reported to interact with KIX domain of CBP/p300 (37). Forkhead domain of FoxO3a intramolecularly interacts with its conserved regions (CR) 3, and binding of forkhead domain to DNA releases CR3, allowing it to bind KIX of CBP/p300 (45). These findings suggest that HBZ interferes in the complex interaction between FoxO3a and CBP/p300, which is likely important to induce apoptosis.

It has been reported that Bim has a tumor-suppressor function in various cancers. Hemizygous loss of the *Bim* gene promoted development of B-cell leukemia in Myc-transgenic mice in which c-myc expression was driven by the immunoglobulin gene intron-enhancer (46). Insulin-like growth factor 1 (IGF-1), an important growth factor for myeloma cells, has been reported to suppress Bim expression by epigenetic and posttranslational mechanisms (25). In Epstein–Barr virus–infected B cells, *Bim* transcription is silenced by DNA methylation of the *Bim* gene promoter (47). Thus, impaired expression of Bim is associated with the various cancers, including the virus-related malignancies. FoxO3a is also a target of oncogenesis. BCR-ABL induces phosphorylation of FoxO3a, which leads to suppressed expression of Bim in $Ph1^+$ chronic myelogenous leukemia cells (32). In breast cancer, IκB kinase interacts with, phosphorylates FoxO3a, which causes proteolysis of FoxO3a (48). In this study, we revealed that HBZ hinders nuclear export of phosphorylated FoxO3a, and impairs function of FoxO3a likely through interaction of FoxO3a and p300. Thus, suppressed Bim and FasL expression through inhibition of FoxO3a by HBZ is a new mechanism for oncogenesis.

Besides FoxO3a perturbation by HBZ, we also have identified the epigenetic aberrations in the promoter region of the *Bim* gene in ATL cells, and found that Bim expression is suppressed by DNA methylation and histone modification. ATL cell lines exhibited upregulated level of H3K27 trimethylation in the promoter regions of *Bim*. It has been reported that enhancer of zeste (EZH) 2, a methyltransferase and component of the polycomb repressive complex 2, expression is increased in ATL cell lines (42). Because EZH2 plays an essential role in the epigenetic maintenance of H3K27 trimethylation, upregulated H3K27 trimethylation of the *Bim* gene promoter might be associated with increased expression of EZH2 in ATL cells. In addition, HBZ seems to be associated with histone deacetylation in MT-1 cells. According to the previous studies, it is known that both HBZ and FoxO3a bind to the histone acetyltransferase p300/CBP through the LXXLL motif (38). In this study, we found that the same motif is important for FoxO3a suppression and resulting inhibition of apoptosis. It is likely that HBZ decreases histone acetylation level on Bim promoter through the interaction with FoxO3a and dissociation of p300/CBP from the promoter. In addition to histone modifications, hypermethylation of CpGs in Bim promoter was observed in some ATL cells. These epigenetic aberrations likely occur as the secondary changes following long-time silencing of *Bim* by HBZ, although further investigations will be required.

Published OnlineFirst October 31, 2013; DOI: 10.1158/0008-5472.CAN-13-0436

In this study, we demonstrated that HBZ suppresses activation-induced apoptosis by downregulation of proapoptotic genes, *Bim* and *FasL*. HBZ perturbs the function of FoxO3a by interaction, and induces epigenetic aberrations in the promoter region of the *Bim* gene. It has been shown that HBZ induces not only cancer but also inflammation *in vivo*. Because inflammatory diseases are essentially caused by failure to negatively regulate unnecessary immune responses by apoptosis, suppression of apoptosis by HBZ might be associated with HTLV-1–induced inflammation as well. Collectively, HBZ-mediated inhibition of apoptosis is likely implicated in both neoplastic and inflammatory diseases caused by HTLV-1.

Disclosure of Potential Conflicts of Interest

No potential conflicts of interest were disclosed.

Authors' Contributions

Conception and design: A. Tanaka-Nakanishi, J. Yasunaga, M. Matsuoka
Development of methodology: A. Tanaka-Nakanishi, M. Matsuoka
Acquisition of data (provided animals, acquired and managed patients, provided facilities, etc.): A. Tanaka-Nakanishi, K. Takai
Analysis and interpretation of data (e.g., statistical analysis, biostatistics, computational analysis): A. Tanaka-Nakanishi, J. Yasunaga, K. Takai, M. Matsuoka
Writing, review, and/or revision of the manuscript: A. Tanaka-Nakanishi, J. Yasunaga, M. Matsuoka
Administrative, technical, or material support (i.e., reporting or organizing data, constructing databases): M. Matsuoka
Study supervision: M. Matsuoka

Acknowledgments

The authors thank T. Furuyama (Kagawa Prefectural University of Health Science) for the 6xDBE-Luc plasmid DNA, P. Bouillet for valuable comments on this study, and L. Kingsbury for proofreading of this manuscript.

Grant Support

This study was supported by a Grant-in-aid for Scientific Research from the Ministry of Education, Science, Sports, and Culture of Japan to M. Matsuoka (MEXT grant number 221S0001), a grant from Japan Leukemia Research Fund to M. Matsuoka, and a grant from the Takeda Science Foundation to J. Yasunaga.

The costs of publication of this article were defrayed in part by the payment of page charges. This article must therefore be hereby marked *advertisement* in accordance with 18 U.S.C. Section 1734 solely to indicate this fact.

Received February 14, 2013; revised September 12, 2013; accepted October 5, 2013; published OnlineFirst October 31, 2013.

References

1. Proietti FA, Carneiro-Proietti AB, Catalan-Soares BC, Murphy EL. Global epidemiology of HTLV-I infection and associated diseases. Oncogene 2005;24:6058–68.
2. Matsuoka M, Jeang KT. Human T-cell leukaemia virus type 1 (HTLV-1) infectivity and cellular transformation. Nat Rev Cancer 2007;7:270–80.
3. Igakura T, Stinchcombe JC, Goon PK, Taylor GP, Weber JN, Griffiths GM, et al. Spread of HTLV-I between lymphocytes by virus-induced polarization of the cytoskeleton. Science 2003;299:1713–6.
4. Pais-Correia AM, Sachse M, Guadagnini S, Robbiati V, Lasserre R, Gessain A, et al. Biofilm-like extracellular viral assemblies mediate HTLV-1 cell-to-cell transmission at virological synapses. Nat Med 2010;16:83–9.
5. Derse D, Hill SA, Lloyd PA, Chung H, Morse BA. Examining human T-lymphotropic virus type 1 infection and replication by cell-free infection with recombinant virus vectors. J Virol 2001;75:8461–8.
6. Mazurov D, Ilinskaya A, Heidecker G, Lloyd P, Derse D. Quantitative comparison of HTLV-1 and HIV-1 cell-to-cell infection with new replication dependent vectors. PLoS Pathog 2010;6:e1000788.
7. Cavrois M, Leclercq I, Gout O, Gessain A, Wain-Hobson S, Wattel E. Persistent oligoclonal expansion of human T-cell leukemia virus type 1-infected circulating cells in patients with Tropical spastic paraparesis/HTLV-1 associated myelopathy. Oncogene 1998;17:77–82.
8. Etoh K, Tamiya S, Yamaguchi K, Okayama A, Tsubouchi H, Ideta T, et al. Persistent clonal proliferation of human T-lymphotropic virus type I-infected cells *in vivo*. Cancer Res 1997;57:4862–7.
9. Grassmann R, Aboud M, Jeang KT. Molecular mechanisms of cellular transformation by HTLV-1 Tax. Oncogene 2005;24:5976–85.
10. Fan J, Ma G, Nosaka K, Tanabe J, Satou Y, Koito A, et al. APOBEC3G generates nonsense mutations in HTLV-1 proviral genomes *in vivo*. J Virol 2010;84:7278–87.
11. Satou Y, Yasunaga J, Yoshida M, Matsuoka M. HTLV-I basic leucine zipper factor gene mRNA supports proliferation of adult T cell leukemia cells. Proc Natl Acad Sci U S A 2006;103:720–5.
12. Satou Y, Yasunaga J, Zhao T, Yoshida M, Miyazato P, Takai K, et al. HTLV-1 bZIP factor induces T-cell lymphoma and systemic inflammation *in vivo*. PLoS Pathog 2011;7:e1001274.
13. Bouillet P, O'Reilly LA. CD95, BIM and T cell homeostasis. Nat Rev Immunol 2009;9:514–9.
14. Debatin KM, Goldman CK, Waldmann TA, Krammer PH. APO-1-induced apoptosis of leukemia cells from patients with adult T-cell leukemia. Blood 1993;81:2972–7.
15. Yasunaga J, Taniguchi Y, Nosaka K, Yoshida M, Satou Y, Sakai T, et al. Identification of aberrantly methylated genes in association with adult T-cell leukemia. Cancer Res 2004;64:6002–9.
16. Krueger A, Fas SC, Giaisi M, Bleumink M, Merling A, Stumpf C, et al. HTLV-1 Tax protects against CD95-mediated apoptosis by induction of the cellular FLICE-inhibitory protein (c-FLIP). Blood 2006;107:3933–9.
17. Okamoto K, Fujisawa J, Reth M, Yonehara S. Human T-cell leukemia virus type-I oncoprotein Tax inhibits Fas-mediated apoptosis by inducing cellular FLIP through activation of NF-kappaB. Genes Cells 2006;11:177–91.
18. Sun SC, Yamaoka S. Activation of NF-kappaB by HTLV-I and implications for cell transformation. Oncogene 2005;24:5952–64.
19. Zhao T, Yasunaga J, Satou Y, Nakao M, Takahashi M, Fujii M, et al. Human T-cell leukemia virus type 1 bZIP factor selectively suppresses the classical pathway of NF-kappaB. Blood 2009;113:2755–64.
20. Brunet A, Bonni A, Zigmond MJ, Lin MZ, Juo P, Hu LS, et al. Akt promotes cell survival by phosphorylating and inhibiting a Forkhead transcription factor. Cell 1999;96:857–68.
21. Zhao T, Satou Y, Sugata K, Miyazato P, Green PL, Imamura T, et al. HTLV-1 bZIP factor enhances TGF-{beta} signaling through p300 coactivator. Blood 2011;118:1865–76.
22. Furuyama T, Nakazawa T, Nakano I, Mori N. Identification of the differential distribution patterns of mRNAs and consensus binding sequences for mouse DAF-16 homologues. Biochem J 2000;349:629–34.
23. Ponchel F, Toomes C, Bransfield K, Leong FT, Douglas SH, Field SL, et al. Real-time PCR based on SYBR-Green I fluorescence: an alternative to the TaqMan assay for a relative quantification of gene rearrangements, gene amplifications and micro gene deletions. BMC Biotechnol 2003;3:18.
24. Richter-Larrea JA, Robles EF, Fresquet V, Beltran E, Rullan AJ, Agirre X, et al. Reversion of epigenetically mediated BIM silencing overcomes chemoresistance in Burkitt lymphoma. Blood 2010;116:2531–42.
25. De Bruyne E, Bos TJ, Schuit F, Van Valckenborgh E, Menu E, Thorrez L, et al. IGF-1 suppresses Bim expression in multiple myeloma via epigenetic and posttranslational mechanisms. Blood 2010;115:2430–40.
26. Fan J, Kodama E, Koh Y, Nakao M, Matsuoka M. Halogenated thymidine analogues restore the expression of silenced genes without demethylation. Cancer Res 2005;65:6927–33.

Published OnlineFirst October 31, 2013; DOI: 10.1158/0008-5472.CAN-13-0436

27. Kumaki Y, Oda M, Okano M. QUMA: quantification tool for methylation analysis. Nucleic Acids Res 2008;36:W170–5.
28. Kino T, De Martino MU, Charmandari E, Ichijo T, Outas T, Chrousos GP. HIV-1 accessory protein Vpr inhibits the effect of insulin on the Foxo subfamily of forkhead transcription factors by interfering with their binding to 14-3-3 proteins: potential clinical implications regarding the insulin resistance of HIV-1-infected patients. Diabetes 2005;54:23–31.
29. Cante-Barrett K, Gallo EM, Winslow MM, Crabtree GR. Thymocyte negative selection is mediated by protein kinase C- and Ca2+-dependent transcriptional induction of bim [corrected]. J Immunol 2006;176:2299–306.
30. Snow AL, Oliveira JB, Zheng L, Dale JK, Fleisher TA, Lenardo MJ. Critical role for BIM in T cell receptor restimulation-induced death. Biol Direct 2008;3:34.
31. Green DR, Droin N, Pinkoski M. Activation-induced cell death in T cells. Immunol Rev 2003;193:70–81.
32. Essafi A, Fernandez de Mattos S, Hassen YA, Soeiro I, Mufti GJ, Thomas NS, et al. Direct transcriptional regulation of Bim by FoxO3a mediates STI571-induced apoptosis in Bcr-Abl-expressing cells. Oncogene 2005;24:2317–29.
33. Busuttil V, Droin N, McCormick L, Bernassola F, Candi E, Melino G, et al. NF-kappaB inhibits T-cell activation-induced, p73-dependent cell death by induction of MDM2. Proc Natl Acad Sci U S A 2010;107:18061–6.
34. Brunet A, Park J, Tran H, Hu LS, Hemmings BA, Greenberg ME. Protein kinase SGK mediates survival signals by phosphorylating the forkhead transcription factor FKHRL1 (FOXO3a). Mol Cell Biol 2001;21:952–65.
35. Obsil T, Obsilova V. Structure/function relationships underlying regulation of FOXO transcription factors. Oncogene 2008;27:2263–75.
36. Modur V, Nagarajan R, Evers BM, Milbrandt J. FOXO proteins regulate tumor necrosis factor-related apoptosis inducing ligand expression. Implications for PTEN mutation in prostate cancer. J Biol Chem 2002;277:47928–37.
37. Wang F, Marshall CB, Yamamoto K, Li GY, Gasmi-Seabrook GM, Okada H, et al. Structures of KIX domain of CBP in complex with two FOXO3a transactivation domains reveal promiscuity and plasticity in coactivator recruitment. Proc Natl Acad Sci U S A 2012;109:6078–83.
38. Clerc I, Polakowski N, Andre-Arpin C, Cook P, Barbeau B, Mesnard JM, et al. An interaction between the human T cell leukemia virus type 1 basic leucine zipper factor (HBZ) and the KIX domain of p300/CBP contributes to the down-regulation of tax-dependent viral transcription by HBZ. J Biol Chem 2008;283:23903–13.
39. Tsai KL, Sun YJ, Huang CY, Yang JY, Hung MC, Hsiao CD. Crystal structure of the human FOXO3a-DBD/DNA complex suggests the effects of post-translational modification. Nucleic Acids Res 2007;35:6984–94.
40. Bouillet P, Zhang LC, Huang DC, Webb GC, Bottema CD, Shore P, et al. Gene structure alternative splicing, and chromosomal localization of pro-apoptotic Bcl-2 relative Bim. Mamm Genome 2001;12:163–8.
41. Gilley J, Ham J. Evidence for increased complexity in the regulation of Bim expression in sympathetic neurons: involvement of novel transcriptional and translational mechanisms. DNA Cell Biol 2005;24:563–73.
42. Gilley J, Coffer PJ, Ham J. FOXO transcription factors directly activate bim gene expression and promote apoptosis in sympathetic neurons. J Cell Biol 2003;162:613–22.
43. Marks P, Rifkind RA, Richon VM, Breslow R, Miller T, Kelly WK. Histone deacetylases and cancer: causes and therapies. Nat Rev Cancer 2001;1:194–202.
44. Fullgrabe J, Kavanagh E, Joseph B. Histone onco-modifications. Oncogene 2011;30:3391–403.
45. Wang F, Marshall CB, Li GY, Yamamoto K, Mak TW, Ikura M. Synergistic interplay between promoter recognition and CBP/p300 coactivator recruitment by FOXO3a. ACS Chem Biol 2009;4:1017–27.
46. Egle A, Harris AW, Bouillet P, Cory S. Bim is a suppressor of Myc-induced mouse B cell leukemia. Proc Natl Acad Sci U S A 2004;101:6164–9.
47. Paschos K, Smith P, Anderton E, Middeldorp JM, White RE, Allday MJ. Epstein-barr virus latency in B cells leads to epigenetic repression and CpG methylation of the tumour suppressor gene Bim. PLoS Pathog 2009;5:e1000492.
48. Hu MC, Lee DF, Xia W, Golfman LS, Ou-Yang F, Yang JY, et al. IkappaB kinase promotes tumorigenesis through inhibition of forkhead FOXO3a. Cell 2004;117:225–37.

nature COMMUNICATIONS

ARTICLE

Received 7 Aug 2013 | Accepted 6 Feb 2014 | Published 26 Feb 2014

DOI: 10.1038/ncomms4393

Loss of NDRG2 expression activates PI3K-AKT signalling via PTEN phosphorylation in ATLL and other cancers

Shingo Nakahata[1,*], Tomonaga Ichikawa[1,*], Phudit Maneesaay[2], Yusuke Saito[1], Kentaro Nagai[1], Tomohiro Tamura[1], Nawin Manachai[1], Norio Yamakawa[1], Makoto Hamasaki[1], Issay Kitabayashi[3], Yasuhito Arai[4], Yae Kanai[5], Tomohiko Taki[6], Takaya Abe[7], Hiroshi Kiyonari[7], Kazuya Shimoda[8], Koichi Ohshima[9], Akira Horii[10], Hiroshi Shima[11], Masafumi Taniwaki[12], Ryoji Yamaguchi[2] & Kazuhiro Morishita[1]

Constitutive phosphatidylinositol 3-kinase (PI3K)-AKT activation has a causal role in adult T-cell leukaemia-lymphoma (ATLL) and other cancers. ATLL cells do not harbour genetic alterations in *PTEN* and *PI3KCA* but express high levels of PTEN that is highly phosphorylated at its C-terminal tail. Here we report a mechanism for the N-myc downstream-regulated gene 2 (NDRG2)-dependent regulation of PTEN phosphatase activity via the dephosphorylation of PTEN at the Ser380, Thr382 and Thr383 cluster within the C-terminal tail. We show that NDRG2 is a PTEN-binding protein that recruits protein phosphatase 2A (PP2A) to PTEN. The expression of *NDRG2* is frequently downregulated in ATLL, resulting in enhanced phosphorylation of PTEN at the Ser380/Thr382/Thr383 cluster and enhanced activation of the PI3K-AKT pathway. Given the high incidence of T-cell lymphoma and other cancers in *NDRG2*-deficient mice, PI3K-AKT activation via enhanced PTEN phosphorylation may be critical for the development of cancer.

[1] Division of Tumor and Cellular Biochemistry, Department of Medical Sciences, University of Miyazaki, 5200 Kihara, Kiyotake, Miyazaki 889-1692, Japan. [2] Department of Veterinary Pathology, University of Miyazaki, Nishi 1-1, Gakuen Kibana Dai, Miyazaki 889-2192, Japan. [3] Division of Hematological Malignancy, National Cancer Center Research Institute, 5-1-1 Tsukiji, Chuo-ku, Tokyo 104-0045, Japan. [4] Division of Cancer Genomics, National Cancer Center Research Institute, 5-1-1 Tsukiji, Chuo-ku, Tokyo 104-0045, Japan. [5] Division of Molecular Pathology, National Cancer Center Research Institute, 5-1-1 Tsukiji, Chuo-ku, Tokyo 104-0045, Japan. [6] Department of Molecular Diagnostics and Therapeutics, Kyoto Prefectural University of Medicine, 465 Kajii-cho, Kawaramachi-Hirokoji, Kamigyo-ku, Kyoto 602-8566, Japan. [7] Laboratory for Animal Resources and Genetic Engineering, RIKEN Center for Developmental Biology, 2-2-3 Minatojima-minamimachi, Chuo-ku, Kobe, Hyogo 650-0047, Japan. [8] Department of Gastroenterology and Hematology, University of Miyazaki, 5200 Kihara, Kiyotake, Miyazaki 889-1692, Japan. [9] Department of Pathology, School of Medicine, Kurume University, 67 Asahimati, Kurume 830-0011, Japan. [10] Department of Molecular Pathology, Tohoku University School of Medicine, 2-1 Seiryo-machi, Aoba-ku, Sendai 980-8575, Japan. [11] Division of Cancer Chemotherapy, Miyagi Cancer Center Research Institute, 47-1 Nodayama, Medeshima-Shiode, Natori 981-1293, Japan. [12] Department of Molecular Hematology and Oncology, Kyoto Prefectural University of Medicine, 465 Kajii-cho, Kawaramachi-Hirokoji, Kamigyo-ku, Kyoto 602-8566, Japan. * These authors contributed equally to this work. Correspondence and requests for materials should be addressed to K.M. (email: kmorishi@med.miyazaki-u.ac.jp).

Adult T-cell leukaemia-lymphoma (ATLL) is an aggressive malignant disease of $CD4^+$ T lymphocytes caused by infection with human T-cell leukaemia virus type 1 (HTLV-1)[1]. HTLV-1 is endemic in many regions, including Japan, the Caribbean and parts of South America, and more than 20 million people are infected with this virus worldwide[2]. ATLL develops in ~5% of infected individuals after a long latency period. Although the viral transactivating protein Tax has a crucial role in the proliferation and transformation of the infected T cells, ATLL cells frequently lose their expression of Tax due to genetic and epigenetic changes in the proviral genome[3]. Another viral product, HBZ, has been shown to support the proliferation of ATLL cells; however, additional cellular events are required for the development of ATLL[3]. Recent studies have shown that the phosphatidylinositol 3-kinase (PI3K)-AKT signalling pathway, one of the major oncogenic pathways, is frequently activated in ATLL and is indispensable for the proliferation of ATLL cells[4,5].

The phosphatase and tensin homologue (PTEN) deleted on the chromosome 10 (*PTEN*) gene was cloned by association with the human cancer susceptibility locus at 10q23 (refs 6,7) and is a lipid phosphatase that dephosphorylates phosphatidylinositol 3,4,5-trisphosphate (PIP_3) to $PI(4,5)P_2$ and opposes the PI3K-AKT pathway, exerting tumour suppressor activity[8]. Although *PTEN* is one of the most frequently mutated genes in human cancer, the frequency of PTEN mutations varies from 1 to 45%[9]. Loss of *PTEN* through genetic alterations can lead to activation of the AKT pathway; however, activation without *PTEN* mutations is likely to occur in the majority of cancers, suggesting that different mechanisms such as *PIK3CA* mutations involve activation of AKT[10]. The lipid phosphatase activity and protein stability of PTEN can be regulated through multiple mechanisms, including acetylation, phosphorylation and ubiquitination[11]. For instance, E3 ubiquitin ligases, NEDD4-1 and WWP2, have been reported to decrease PTEN stability by catalysing PTEN poly-ubiquitination, and the PTEN degradation predisposes to tumourigenesis[12–14]. In addition, PTEN is subject to phosphorylation at the C-terminal serine–threonine cluster (Ser370, Ser380, Thr382, Thr383 and Ser385) that affects its phosphatase activity, subcellular localization and protein stability[15–17]. It has been proposed that phosphorylation of the C-terminal sites keeps PTEN in an inactive form in the cytoplasm; however, the dephosphorylation induces translocation of PTEN to the plasma membrane where the active PTEN antagonizes PI3K-AKT signalling[18]. PTEN inactivation through increased phosphorylation of the C-terminal serine–threonine cluster is observed in several malignancies, including T-cell acute lymphoblastic leukaemia (T-ALL)[19,20], and casein kinase II (CK2) has been proposed as a candidate protein kinase for the phosphorylation at these sites[21]. However, the molecular mechanisms responsible for this hyperphosphorylation remain poorly understood.

Here we identify N-myc downstream-regulated gene 2 (NDRG2) as a PTEN-associated protein that recruits protein phosphatase 2A (PP2A) to facilitate dephosphorylation of PTEN at the Ser380, Thr382 and Thr383 cluster. Our results indicate that genetic and epigenetic inactivation of *NDRG2* in ATLL cells leads to increased phosphorylation of PTEN, resulting in decreased PTEN lipid phosphatase activity and subsequent enhanced activation of the PI3K-AKT pathway. Moreover, *NDRG2*-deficient mice show high levels of AKT phosphorylation in various tissues and spontaneous tumour development of various types, including T-cell lymphomas, providing the first *in vivo* evidence that *NDRG2* functions as a tumour suppressor gene. Because downregulation of *NDRG2* is reported in several types of cancers, the phosphorylation of PTEN at the Ser380/Thr382/Thr383 cluster via *NDRG2* inactivation is one of the most important events leading to the dysregulation of PTEN function in cancer.

Results

***NDRG2* is a candidate tumour suppressor gene in ATLL.** We recently mapped 605 chromosomal breakpoints in 61 ATLL cases by spectral karyotyping and identified chromosome 14q11 as one of the most common chromosomal breakpoint regions[22]. To map the precise location of the 14q11 chromosomal breakpoints, we performed single-nucleotide polymorphism (SNP)-based comparative genomic hybridization on leukaemia cells from acute-type ATLL patients. In patients with chromosomal deletions at 14q11, the breakpoints frequently accumulated adjacent to the T-cell receptor alpha–delta chain locus (*TCRα/δ*), and a recurrent 0.9-Mb interstitial deletion was identified in a region including part of the *TCRα/δ* locus (Fig. 1a). Because tumour suppressors and oncogenes are commonly located at fragile sites[23], we analysed the expression of the 25 genes that map within the 0.9-Mb region in ATLL cells from seven acute-type ATLL patients and in $CD4^+$ T lymphocytes from the peripheral blood of five healthy volunteers (references) using oligonucleotide microarrays (Supplementary Methods) (Affymetrix U133 Plus 2.0). *NDRG2*, a member of a new family of differentiation-related genes[24], and TCR delta variable 3 (*TRDV3*) were consistently downregulated in all seven ATLL samples compared with the five normal control samples from healthy volunteers (Fig. 1a). Furthermore, we used a genome-wide DNA methylation analysis in combination with microarray gene expression analysis to identify genes that are frequently methylated and silenced in ATLL. We identified 34 genes including *NDRG2* that become methylated and transcriptionally repressed during ATLL leukaemogenesis (Supplementary Table 1, Supplementary Methods). Here, we investigated whether *NDRG2* might be a 14q11 tumour suppressor candidate in ATLL. Quantitative reverse transcription-PCR (RT-PCR) analysis confirmed that *NDRG2* expression was significantly reduced in a series of ATLL cell lines and primary acute-type ATLL samples when compared with HTLV-1-negative T-ALL cell lines and $CD4^+$ lymphocytes from healthy volunteers, respectively (Fig. 1b). Treatment with an inhibitor of histone deacetylase, trichostatin A, and/or an inhibitor of DNA methylation, 5-aza-deoxycytidine, restored the expression of *NDRG2* in most of the ATLL cell lines (Supplementary Fig. 1), suggesting that epigenetic modification is an important mechanism to reduce the expression of *NDRG2* in ATLL cells. In accordance with DNA methylation array data, the CpG islands of the *NDRG2* promoter were heavily methylated in three ATLL cell lines and primary ATLL cells from five acute-type ATLL patients, but not in three T-ALL cell lines and control $CD4^+$ lymphocytes from five healthy volunteers, as revealed by bisulfite-sequencing analysis (Supplementary Fig. 2). Similarly, a methylation-specific PCR confirmed the hypermethylation of the *NDRG2* promoter in the majority of ATLL cells (eight of eight ATLL cell lines and 34 of 34 primary samples) (Supplementary Table 2). No somatic mutations in the *NDRG2* gene were observed in 34 primary ATLL samples and 42 cancer cell lines, including eight ATLL cell lines (Supplementary Table 3), except for previously reported SNPs (Supplementary Table 4). These data indicated that *NDRG2* is frequently inactivated by genomic deletion and epigenetic silencing in ATLL.

The PI3K-AKT signalling pathway is activated in ATLL cells. Because the PI3K-AKT signalling pathway is constitutively activated in ATLL cells[4], we analysed PTEN and NDRG2 expression and the activation status of PI3K-AKT in primary ATLL cells from acute-type ATLL patients and in ATLL cell lines (Fig. 2a,b).

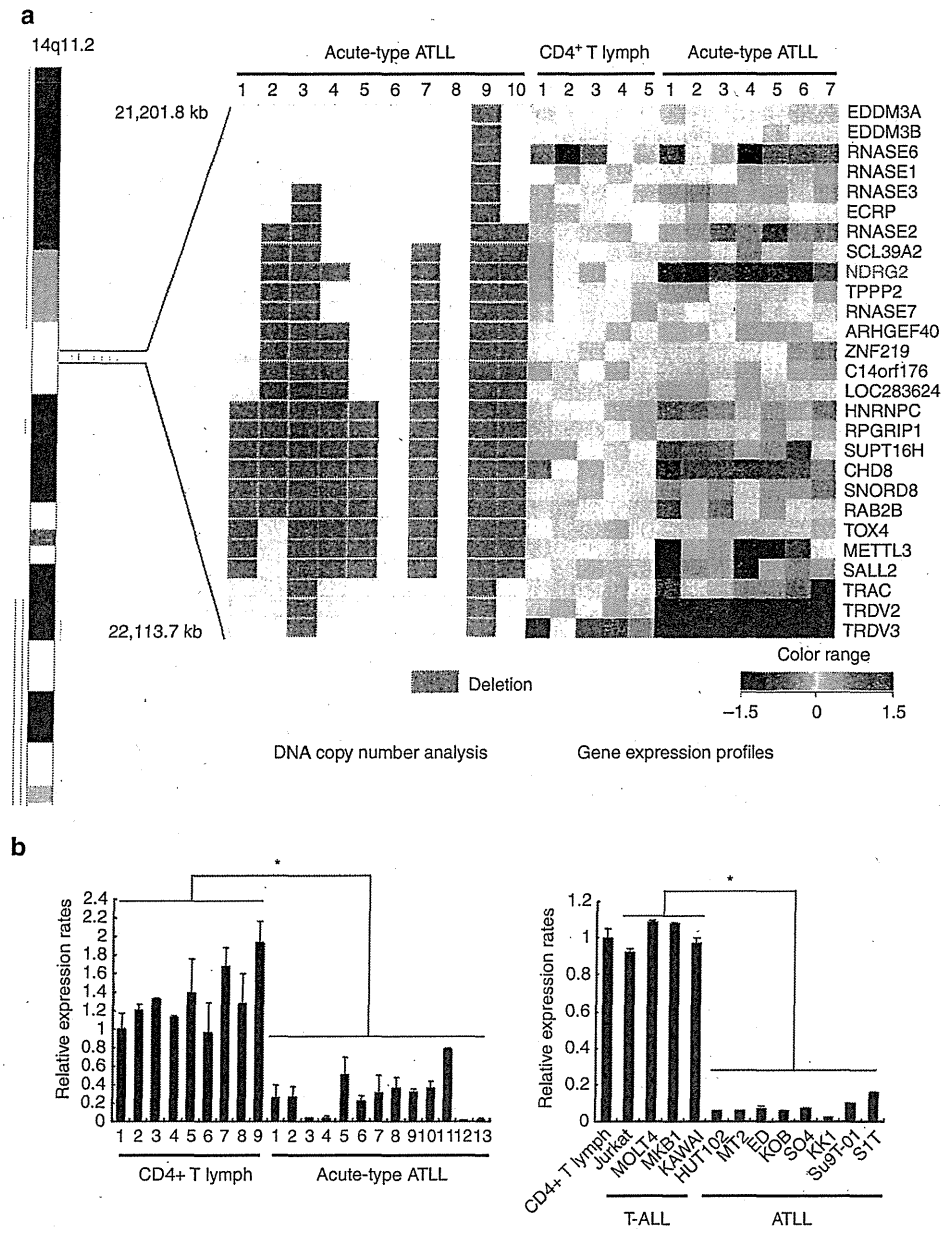

Figure 1 | *NDRG2* is a candidate tumour suppressor gene in ATLL. (**a**) Genomic and gene expression analysis of chromosome 14q11. Results from the SNP array-based comparative genomic hybridization (CGH) analysis on chromosome 14 in ten samples from acute-type ATLL patients. Green bars represent loss of copy number and red bars represent gain of copy number. Out of the ten ATLL samples, eight had breakpoints on 14q11 clustered in a region of 0.9 Mb between genomic positions 21,201,800 and 22,113,700. A heatmap of the normalized gene expression measures for the 27 genes mapped to the recurrent breakpoint region in the CD4$^+$ T lymphocytes from five healthy volunteers and ATLL cells from seven acute-type ATLL patients is shown with the deletion map, in which columns represent samples and rows represent genes. A gradient of blue and red colours represent low- and high-relative fold changes of gene expression to the average expression in normal controls. Genes with average signal intensities less than 100 were eliminated. (**b**) Expression of *NDRG2* mRNA in ATLL cells. Quantitative RT-PCR analysis of *NDRG2* was performed with mRNA isolated from nine samples of CD4$^+$ T lymphocytes from healthy volunteers and 13 samples of ATLL cells from the patients, along with samples from four T-ALL cell lines and eight ATLL cell lines. The relative amounts of mRNA were normalized against β-actin mRNA and expressed relative to the mRNA abundance in healthy control sample 1. Mean ± s.d. is shown, *$P<0.05$ (Mann–Whitney *U*-test). More than a 50% reduction in *NDRG2* mRNA expression was observed in 12 out of 13 cases (92%) of ATLL. Data are representative of two experiments.

The NDRG2 protein expression in ATLL cell lines and primary ATLL cells was significantly lower than that in T-ALL cell lines and CD4$^+$ lymphocytes from healthy volunteers, and AKT phosphorylation at Ser473 and Thr308, an indicator of AKT activation, was detected in the majority of the primary ATLL samples and ATLL cell lines. Because *PTEN* mRNA and protein were expressed at normal levels in all of the ATLL samples except the SO4 cell line (Fig. 2c), we performed a mutation analysis of the *PTEN* and *PIK3CA* genes. No mutations were detected within the coding and adjacent intronic regions of *PTEN* or in the hotspot mutation regions of *PIK3CA* in the ATLL samples (Supplementary Table 3). Therefore, we considered the possibility

that post-translational modifications of PTEN influence PTEN phosphatase activity in ATLL cells. The phosphorylation of PTEN at the serine–threonine cluster (Ser370, Ser380, Thr382, Thr383 and Ser385) in the C-terminal tail suppresses its phosphatase activity[17]; therefore, we evaluated PTEN phosphorylation and demonstrated that the cluster sites were highly phosphorylated in the primary ATLL cells and ATLL cell lines, whereas the non-phosphorylated form was lower in abundance compared with controls (Fig. 2a,b; Supplementary Fig. 3). Notably, we also found that the SO4 cell line, which has a higher level of PTEN expression, contains high levels of phosphorylated PTEN and an elevated level of phosphorylated AKT (Supplementary Fig. 4). Furthermore, the expression levels of SHIP1, a different class of lipid phosphatase that catalyses PIP_3 to $PI(3,4)P_2$ (ref. 25),

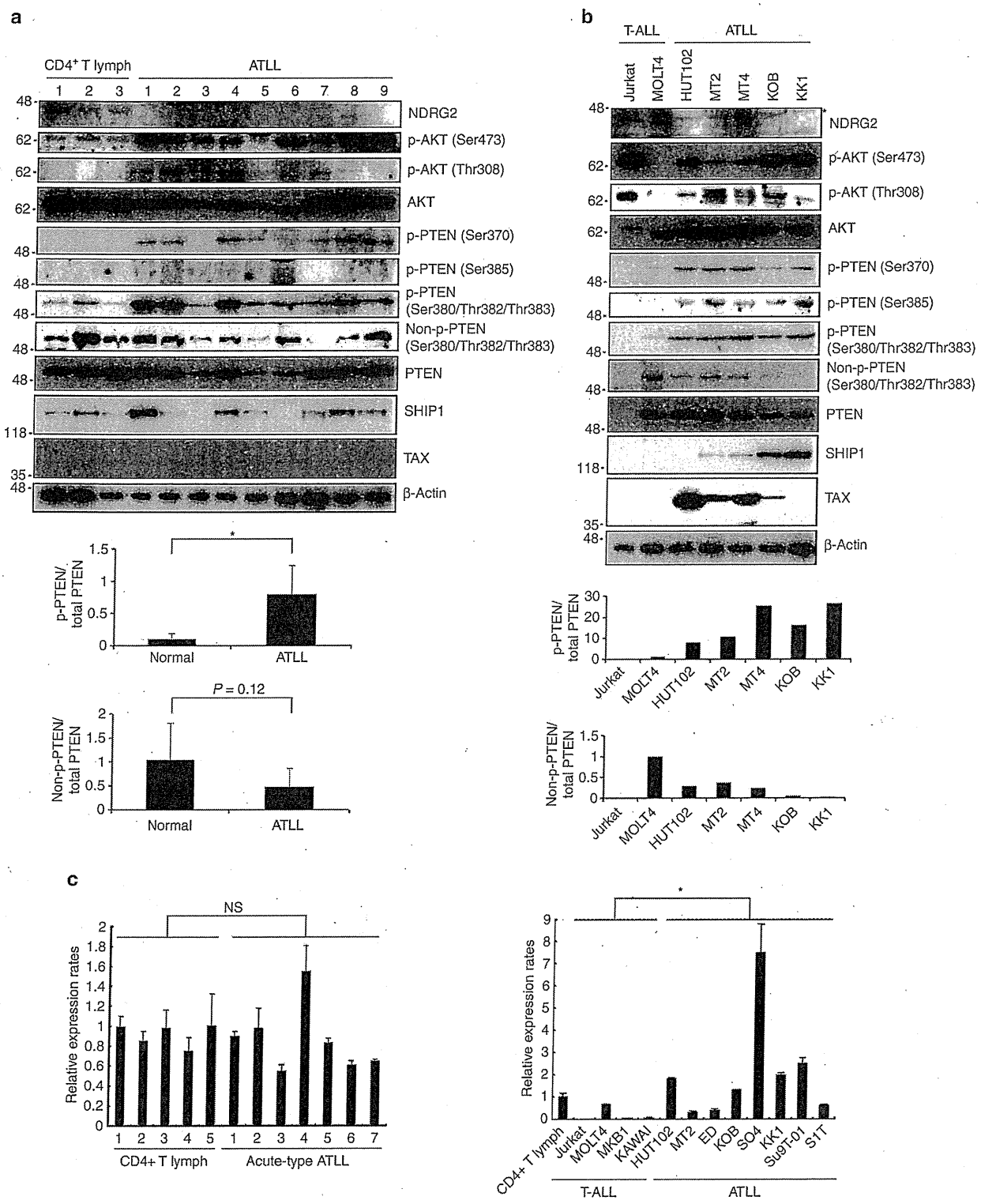

showed no significant differences between ATLL cells and controls, although a few cases showed higher levels of SHIP1 (Fig. 2a,b). Collectively, these results suggested that PI3K-AKT pathway activation in ATLL may be related to increased PTEN phosphorylation and potentially to the inactivation of *NDRG2*.

NDRG2 expression induces dephosphorylation of PTEN and AKT. To determine whether low NDRG2 expression was associated with increased PTEN phosphorylation and PI3K-AKT activation in ATLL cells, we introduced an NDRG2 expression vector into two ATLL cell lines (KK1 and HUT102). The phosphorylation of AKT-Ser473 and PTEN-Ser380/Thr382/Thr383, but not PTEN-Ser370 and PTEN-Ser385, was markedly decreased in both NDRG2-expressing cell lines (Fig. 3a; Supplementary Fig. 5a), although NDRG2 expression did not significantly change the basal activity of PI3K (Supplementary Fig. 6). There was also an increase in the abundance of Ser380/Thr382/Thr383 non-phosphorylated PTEN in NDRG2-expressing cells (Supplementary Fig. 7). No change in SHIP1 expression was detected (Fig. 3a). In addition, the NDRG2-transfected cells exhibited decreased growth rates and a predominant nuclear localization of forkhead box protein O1 and O4 (FOXO1/4) (a marker of low AKT activity status) (Fig. 3b,c; Supplementary Fig. 5b). Furthermore, to determine whether NDRG2 expression may influence the tumour growth of transplanted ATLL cells *in vivo*, mock vector-transfected or NDRG2-transfected KK1 cells were injected intravenously into NOD/Shi-*scid*, interleukin (IL)-2Rg^{null} (NOG) mice. The average duration of life of 10 mice after inoculation with KK1-Mock cells was 67 days, but that of 10 mice inoculated with KK1-NDRG2 cells was extended to 207 days (Fig. 3d; Supplementary Fig. 8). Statistically significant difference in apoptotic cell rate was also found in the infiltrating neoplastic cells between KK1-Mock- and KK1-NDRG2-injected mice (Supplementary Fig. 9). To investigate these observations further, we performed the reverse experiment by inhibiting NDRG2 expression in the MOLT4 cell line. Transfection of the MOLT4 cell line with short hairpin RNA (shRNA) against NDRG2 enhanced the phosphorylation of PTEN-Ser380/Thr382/Thr383 and AKT-Ser473, which was accompanied by increased cell proliferation and a relocation of FOXO1/4 from the nucleus to the cytoplasm (Fig. 3e–g). We utilized the NIH3T3 mouse embryonic fibroblast cell line to confirm whether NDRG2 expression attenuates PTEN-Ser380/Thr382/Thr383 phosphorylation and AKT activation. After serum stimulation or transfection of a constitutively active PI3K mutant, we determined that the inhibition of *NDRG2* expression resulted in increases in phosphorylated PTEN-Ser380/Thr382/Thr383 and AKT-Ser473 compared with the control cells (Supplementary Figs 10 and 11). In contrast, the forced expression of NDRG2 in NIH3T3 cells resulted in a dose-dependent decrease in PTEN-Ser380/Thr382/Thr383 and AKT-Ser473 phosphorylation under conventional culture conditions (Supplementary Fig. 12). To establish a direct link between PTEN-Ser380/Thr382/Thr383 phosphorylation and PI3K-AKT activation, we constructed PTEN-S370A, -S380A/T382A/T383A and -S385A mutants in which Ser370, a Ser380/Thr382/Thr383 cluster and Ser385, respectively, were replaced with alanines. The forced expression of the PTEN-S380A/T382A/T383A mutant in HUT102 cells decreased AKT phosphorylation, cell growth and nuclear localization of FOXO1/4, whereas the expression of the PTEN-S370A or PTEN-S385A mutant had no significant effect (Fig. 3h–j). Treatment of ATLL cells with the CK2 inhibitors, 4,5,6,7-tetrabromobenzotriazole (TBB) and CX-4945, did not change the level of phosphorylated PTEN-Ser380/Thr382/Thr383, whereas the same treatment decreased PTEN-Ser370, a bona fide CK2 substrate[26], and AKT-Ser473 phosphorylation (Supplementary Fig. 13). These results indicate that the phosphorylation on PTEN-Ser380/Thr382/Thr383 has an important role in the activation of PI3K-AKT in ATLL cells, and that NDRG2 is able to reverse PTEN-Ser380/Thr382/Thr383 phosphorylation, leading to the suppression of PI3K-AKT activation.

NDRG2 is a novel PTEN-interacting protein. To determine whether NDRG2 physically associates with PTEN, lysates from KK1 cells stably expressing FLAG-tagged NDRG2 were immunoprecipitated with an anti-FLAG antibody, and NDRG2-associated proteins were analysed by western blotting with a PTEN-specific antibody. We found that ectopically expressed NDRG2 co-precipitated with endogenous PTEN in ATLL cells (Fig. 4a). Exogenously expressed green fluorescent protein (GFP)-tagged PTEN and FLAG-tagged NDRG2 co-precipitated in 293T cells (Fig. 4b), and endogenous NDRG2 and PTEN co-immunoprecipitated with each specific antibody and co-localized in the cytoplasm in MOLT4 cells (Fig. 4c,d), suggesting that these two proteins physically interact in T lymphocytes. By subjecting a series of deletion mutants to co-immunoprecipitation assays, a domain containing a putative α–β hydrolase fold (NDR domain) that is conserved among NDRG family members[27] was found to interact with the C-terminal half of PTEN, which contains a C2 lipid-binding domain (Supplementary Fig. 14). In addition, the S370A, S380A/T382A/T383A and S385A mutations in PTEN did not significantly interfere with the binding of NDRG2 (Supplementary Fig. 15), suggesting that NDRG2 can bind to both the phosphorylated and non-phosphorylated forms of PTEN.

NDRG2 recruits PP2A to dephosphorylate PTEN. To determine the mechanism by which NDRG2 expression induces PTEN dephosphorylation, we incubated KK1-NDRG2 cell lysates with a synthetic PTEN phosphopeptide containing the Ser380/Thr382/

Figure 2 | The PI3K-AKT signalling pathway is activated in ATLL cells. (**a**) A western blot analysis of NDRG2, PTEN, phosphorylated PTEN (p-PTEN) (Ser370, Ser380/Thr382/Thr383 and Ser385), non-p-PTEN (Ser380/Thr382/Thr383), SHIP1, AKT, p-AKT (Ser473 and Thr308) and Tax was performed in primary leukaemic cells from acute-type ATLL patients. The CD4$^+$ T lymphocytes from healthy volunteers (CD4$^+$ T lymph) served as the controls. No expression of Tax was detected in CD4$^+$ T lymphocytes from healthy volunteers or ATLL cells from acute-type ATLL patients. The graph shows relative band intensity of p-PTEN (Ser380/Thr382/Thr383) and non-p-PTEN (Ser380/Thr382/Thr383). Each p-PTEN or non-p-PTEN value was divided by the total PTEN value for a given sample. The data are expressed as the mean value ± s.d. (*$P<0.05$, Student's *t*-test). The data are representative of three experiments. (**b**) A western blot analysis with the same antibodies as in Fig. 2a was performed in the T-ALL and ATLL cell lines. Asterisk, nonspecific band. HTLV-1-transformed T-cell lines (HUT102, MT2 and MT4) expressed high levels of Tax. The graph shows relative band intensity of p-PTEN (Ser380/Thr382/Thr383) and non-p-PTEN (Ser380/Thr382/Thr383). Each p-PTEN or non-p-PTEN value was divided by the total PTEN value for a given sample. The data are representative of three experiments. (**c**) Quantitative RT-PCR analysis of *PTEN* in CD4$^+$ T lymphocytes from five healthy volunteers and ATLL cells from seven acute-type ATLL patients, along with four T-ALL cell lines and eight ATLL cell lines. The relative amounts of mRNA were normalized against β-actin mRNA and expressed relative to the mRNA abundance in healthy control sample 1. The mean ± s.d. is shown; *$P<0.05$; NS, not significant (Mann–Whitney *U*-test). The data are representative of two experiments.

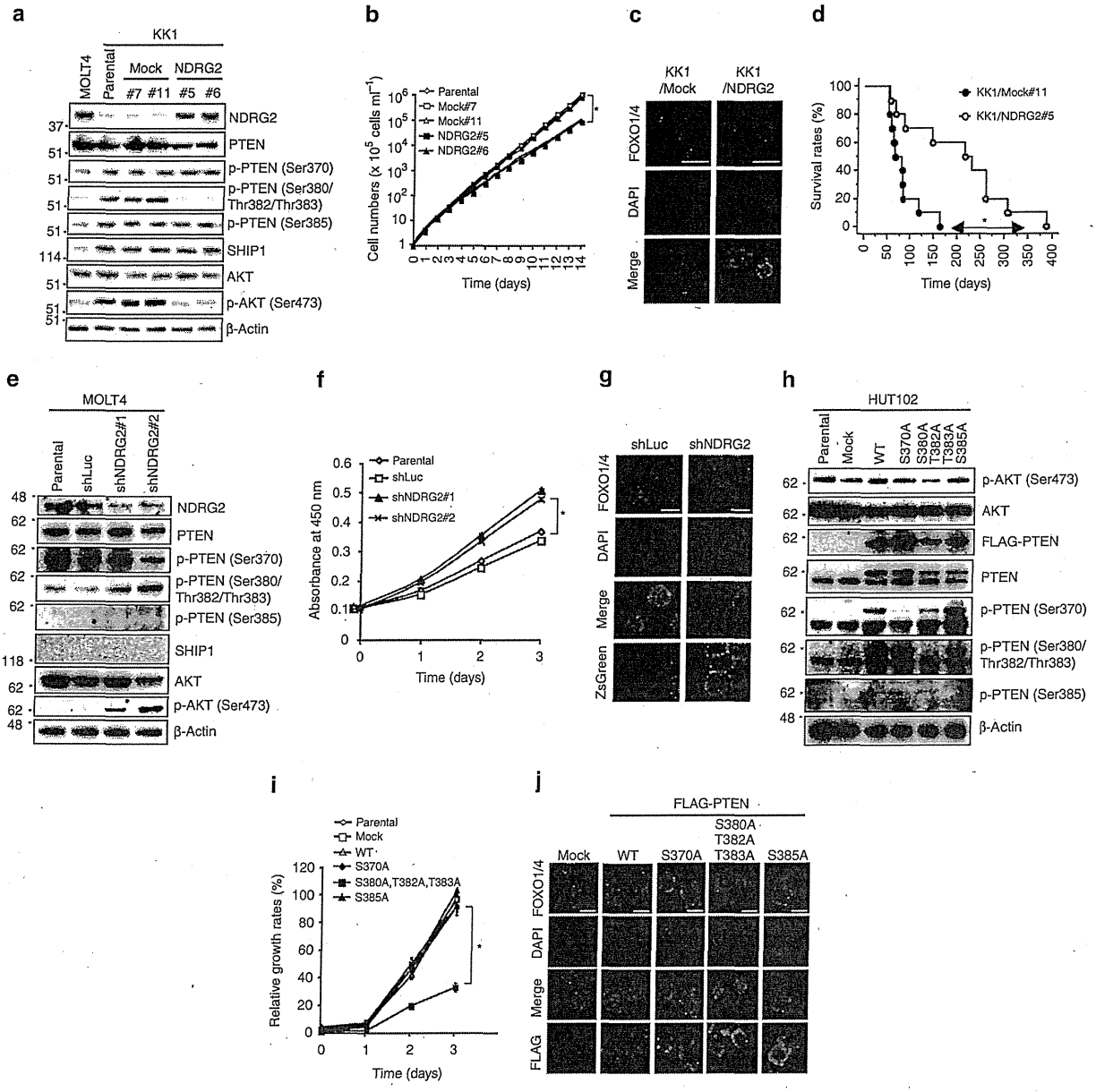

Figure 3 | Decreased expression of *NDRG2* and the enhanced phosphorylation of PTEN are involved in the activation of PI3K-AKT. (**a**) Western blots analysis of stably transfected KK1 cells. Note that the amount of NDRG2 protein in both MOLT4 and NDRG2-transfected KK1 cells was found to be similar. The data are representative of three experiments. (**b**) The proliferation rates of KK1-NDRG2, KK1-Mock, and parental KK1 cells. The mean ± s.d. is shown; $^*P<0.05$ (Student's *t*-test). The data are representative of three experiments. (**c**) The subcellular localization of FOXO1/4 in KK1-NDRG2 and KK1-Mock cells. The nuclei were labelled with DAPI. Scale bar, 10 μm. The data are representative of three experiments. (**d**) Kaplan–Meier survival curves of NOG mice intravenously injected with KK1-NDRG2 or KK1-Mock cells ($n=10$ mice per group, $^*P<0.05$, log-rank test). (**e**) MOLT4 cells transiently transfected with two different shRNAs against NDRG2 or control shRNA against luciferase (shLuc) were subjected to western blotting. The data are representative of three experiments. (**f**) The proliferation rates of MOLT4 cells transfected with shNDRG2 or shLuc expression vectors. The mean ± s.d. is shown; $^*P<0.05$ (Student's *t*-test). The data are representative of three experiments. (**g**) The subcellular localization of FOXO1/4 in MOLT4 cells transfected with shNDRG2 or shLuc. The transfected cells were visualized by ZsGreen expression. Scale bar, 10 μm. The data are representative of three experiments. (**h**) HUT102 cells transfected with WT PTEN or PTEN mutants were subjected to western blotting. A slower migrating band for PTEN and phosphorylated PTEN appears in the presence of transfected PTEN, and a high level of phosphorylation of exogenous PTEN-Ser380/Thr382/Thr383 was observed in HUT102 cells. The data are representative of three experiments. (**i**) The proliferation rates of HUT102 cells transfected with WT or mutant PTEN. The mean ± s.d. is shown; $^*P<0.05$ (Student's *t*-test). The data are representative of three experiments. (**j**) The subcellular localization of FOXO1/4 in HUT102 cells transfected with WT or mutant PTEN. The transfected cells were visualized using an antibody against FLAG. Scale bar, 10 μm. The data are representative of three experiments.

Thr383 cluster in the presence or absence of increasing concentrations of okadaic acid (OA), an inhibitor of the serine–threonine phosphatases, PP1 and PP2A[28]. We incubated KK1/NDRG2 cell lysates with the synthetic pSer380/pThr382/pThr383 peptide in the presence or absence of increasing concentrations of OA. As expected, the phosphatase activity in

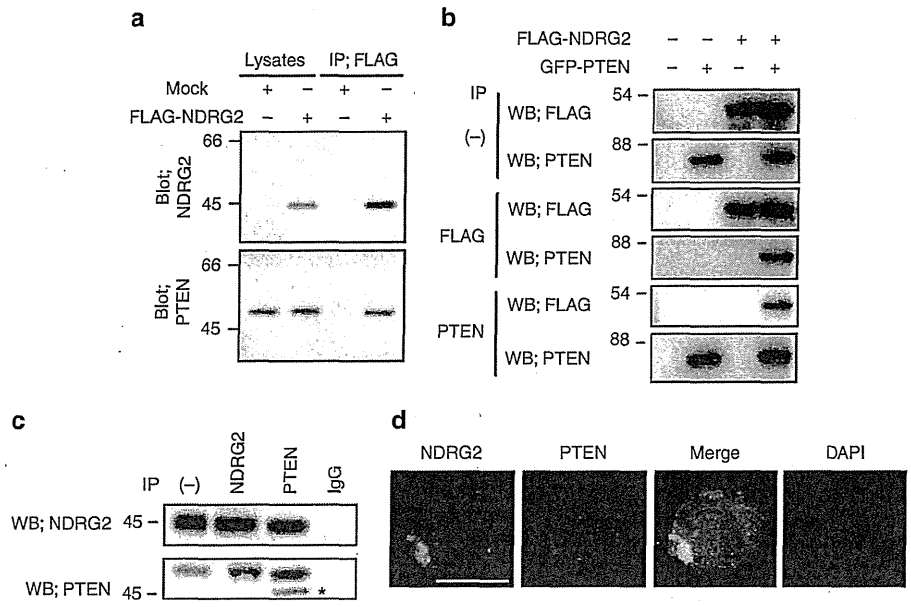

Figure 4 | NDRG2 is a novel PTEN-interacting protein. (**a**) The KK1 cell lysates transfected with the mock or FLAG-NDRG2 vector were immunoprecipitated with an anti-FLAG antibody, and the western blots were probed with the indicated antibodies. IP, immunoprecipitation. The data are representative of three experiments. (**b**) Exogenously expressed PTEN and NDRG2 were co-immunoprecipitated in 293T cells (WB, western blot). The data are representative of three experiments. (**c**) The co-immunoprecipitation of endogenous PTEN and NDRG2 was performed in MOLT4 cell lysates. On the input lane (–), 1/200 of the input was loaded for detection of NDRG2. Asterisk, nonspecific band. The data are representative of three experiments. (**d**) The co-localization of endogenous PTEN and NDRG2 was determined in MOLT4 cells. The nuclei were labelled with DAPI. Scale bar, 10 μm. The data are representative of three experiments.

KK1-NDRG2 cell lysates was substantially inhibited by a low concentration of OA (10 nM) (Fig. 5a). In addition, the dephosphorylation of PTEN-Ser380/Thr382/Thr383 in KK1-NDRG2 cells was inhibited by OA in a dose-dependent manner (Fig. 5b), but there was no effect on PTEN-Ser370 phosphorylation. In accordance with these results, a transiently expressed PP2A catalytic subunit (PP2Ac), but not PP1c or PP5c, efficiently dephosphorylated the synthetic pSer380/pThr382/pThr383 peptide, which was prevented by 10 nM OA (Fig. 5c; Supplementary Fig. 16). Similarly, the endogenous PP2Ac immunoprecipitated from NIH3T3 lysates exhibited phosphatase activity toward the pSer380/pThr382/pThr383 peptide in an OA-sensitive manner (Fig. 5d; Supplementary Fig. 17). In support of these data, small interfering RNA (siRNA)-mediated knockdown of PP2Acα prevented the NDRG2-dependent PTEN dephosphorylation in KK1-NDRG2 cells (Supplementary Fig. 18). Further analysis revealed that the recombinant PP2A core enzyme, a dimer of PP2Ac and the structural A subunit, also dephosphorylated the pSer380/pThr382/pThr383 peptide and was capable of dephosphorylating each of the three phosphorylated residues (pSer380, pThr382 and pThr383) with comparable efficiencies (Fig. 5e). Recombinant PP2A dephosphorylated PTEN-Ser380/Thr382/Thr383 purified from KK1 cell lysates (Fig. 5f), indicating that PP2A specifically mediates the dephosphorylation of PTEN-Ser380/Thr382/Thr383. We demonstrated that PP2Ac co-precipitated with NDRG2 in the lysates of crosslinked HUT102/NDRG2 cells (Fig. 5g). Although PP2Ac was barely detectable in the PTEN immunoprecipitates from KK1-Mock cells (Fig. 5h), PTEN clearly co-precipitated with both NDRG2 and PP2Ac in KK1-NDRG2 cells; this result was accompanied by decreased PTEN-Ser380/Thr382/Thr383 phosphorylation (Fig. 5h), suggesting that NDRG2 recruits PP2A to PTEN and thereby promotes PTEN-Ser380/Thr382/Thr383 dephosphorylation. Remarkably, we found that C-terminal deletion mutants of NDRG2 (ΔC and NDR), which do not interact with PP2A, are impaired in their ability to downregulate PTEN-Ser380/Thr382/Thr383 phosphorylation (Supplementary Fig. 19).

***NDRG2*-deficient mice are susceptible to spontaneous tumours.** To determine whether NDRG2 has a role in tumourigenesis, we generated *NDRG2*-deficient (*NDRG2*$^{-/-}$) mice (Supplementary Fig. 20), which were born at normal Mendelian ratios (Supplementary Table 5) and developed without apparent physical abnormalities. NDRG2 was highly expressed in the adult mouse brain, heart and liver[29] (Fig. 6a). The mutant mice exhibited increased levels of phosphorylated PTEN-Ser380/Thr382/Thr383, AKT-Ser473 and GSK3β-Ser9 in all of the tissues examined (Fig. 6b). In addition to the NDRG2 and PTEN interaction in the frontal cortex of wild-type (WT) mice (Fig. 6c), the *NDRG2*$^{-/-}$ embryonic fibroblasts exhibited increased phosphorylated PTEN-Ser380/Thr382/Thr383, high AKT-Ser473 phosphorylation and an accelerated cell proliferation rate (Fig. 6d,e). The *NDRG2*$^{-/-}$ mice had a markedly shorter lifespan than the WT or *NDRG2*$^{+/-}$ mice (Fig. 6f), and they developed various types of tumours, including lymphoma, hepatocellular carcinoma and bronchoalveolar carcinoma (Supplementary Table 6; Fig. 6g,h). Malignant lymphomas occurred at a high frequency (~50%), and the infiltrating lymphoid cells were $CD3^+CD4^+CD8^-$, indicating a mature helper T-cell phenotype (Fig. 6i–n; Supplementary Fig. 21), suggesting that NDRG2 is a possible tumour suppressor in various types of cancer, including peripheral T-cell lymphoma.

***NDRG2* downregulation activates PI3K-AKT in various cancers.** We next evaluated the methylation status of the *NDRG2* promoter in various cancer cell lines from different organ origins.

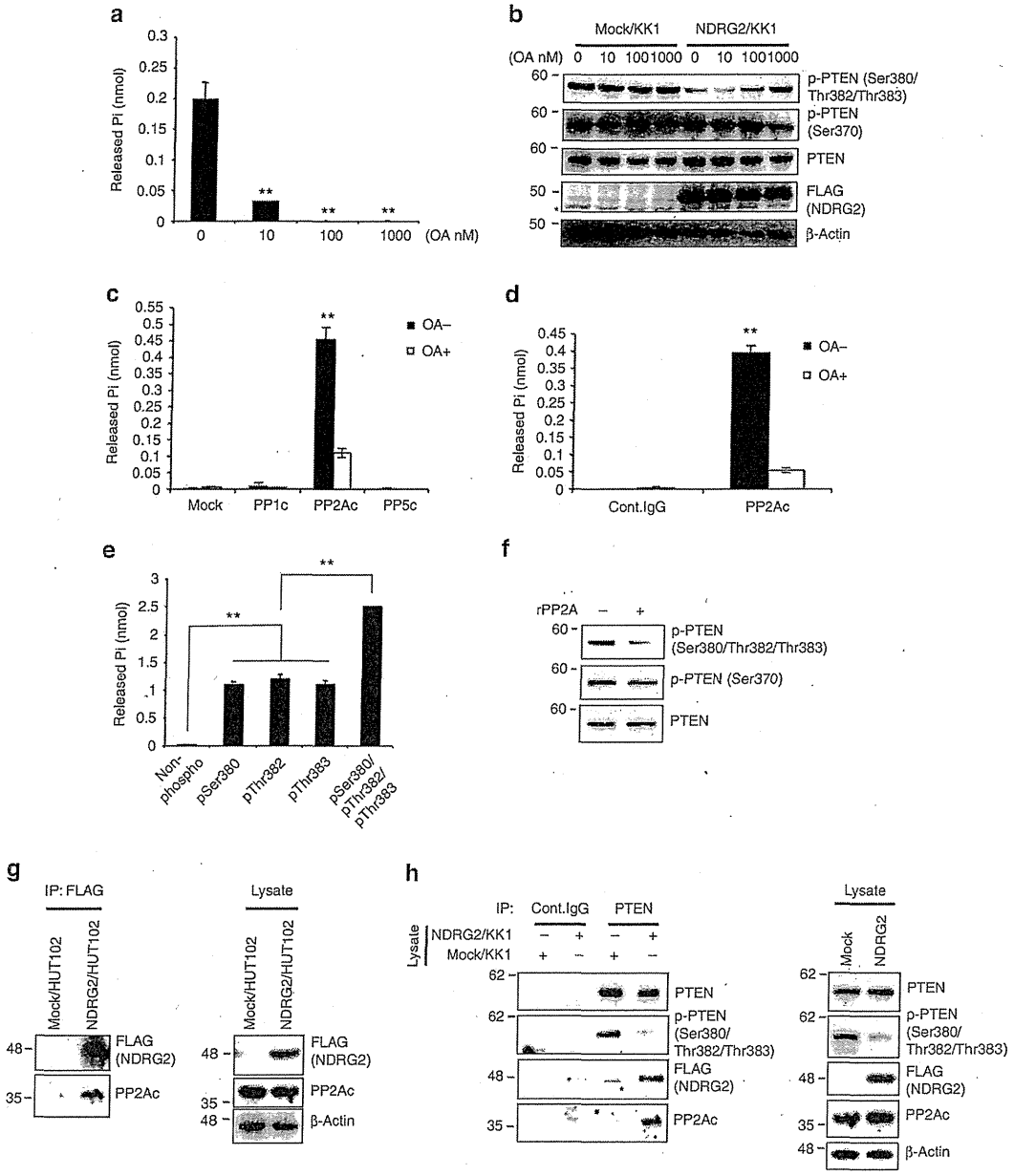

Figure 5 | NDRG2 recruits PP2A to PTEN leading to its dephosphorylation at pSer380/pThr382/pThr383. (**a**) KK1-NDRG2 cell lysates were incubated with a pSer380/pThr382/pThr383 PTEN phosphopeptide in the presence or absence of different concentrations of OA. The amount of released phosphate was quantitated using the malachite green assay. The mean ± s.d. is shown; $^{**}P<0.05$ compared with untreated control (Student's *t*-test). The data are representative of three experiments. (**b**) KK1-Mock and KK1-NDRG2 cells were treated with increasing concentrations of OA for 2 h and subjected to western blot analysis. Asterisk, nonspecific band. The data are representative of three experiments. (**c**) After immunoprecipitating lysates from 293T cells transfected with the indicated vectors, the beads were incubated with a pSer380/pThr382/pThr383 phosphopeptide in the presence or absence of 10 nM OA, and phosphate release was determined. The mean ± s.d. is shown; $^{**}P<0.05$ (Student's *t*-test). The data are representative of three experiments. (**d**) After immunoprecipitating the NIH3T3 lysates with an anti-PP2Ac antibody, the beads were incubated with a pSer380/pThr382/pThr383 phosphopeptide in the presence or absence of 10 nM OA, and phosphate release was determined. The mean ± s.d. is shown; $^{**}P<0.05$ (Student's *t*-test). The data are representative of three experiments. (**e**) 0.5 unit of recombinant PP2A was incubated with 200 μg ml^{-1} of either PTEN peptide or the phosphopeptides containing either pSer380, pThr382, pThr383 or pSer380/pThr382/pThr383, and phosphate release was determined. The mean ± s.d. is shown; $^{**}P<0.05$ (Student's *t*-test). The data are representative of three experiments. (**f**) The beads were incubated with or without recombinant PP2A after immunoprecipitating the KK1-Mock lysates with an anti-PTEN antibody. Western blot analysis of the reaction mixtures was performed to determine the degree of phosphorylation of PTEN. The data are representative of two experiments. (**g**) The lysates of HUT102-NDRG2 or HUT102-Mock cells treated with the crosslinker DTBP were immunoprecipitated with an anti-FLAG antibody and subsequently probed for co-precipitated PP2Ac by Western blotting. The data are representative of three experiments. (**h**) The lysates from KK1-NDRG2 or KK1-Mock cells treated with DTBP were immunoprecipitated with an anti-PTEN antibody, and the Western blots were probed with the indicated antibodies. Asterisk, nonspecific band. The data are representative of three experiments.

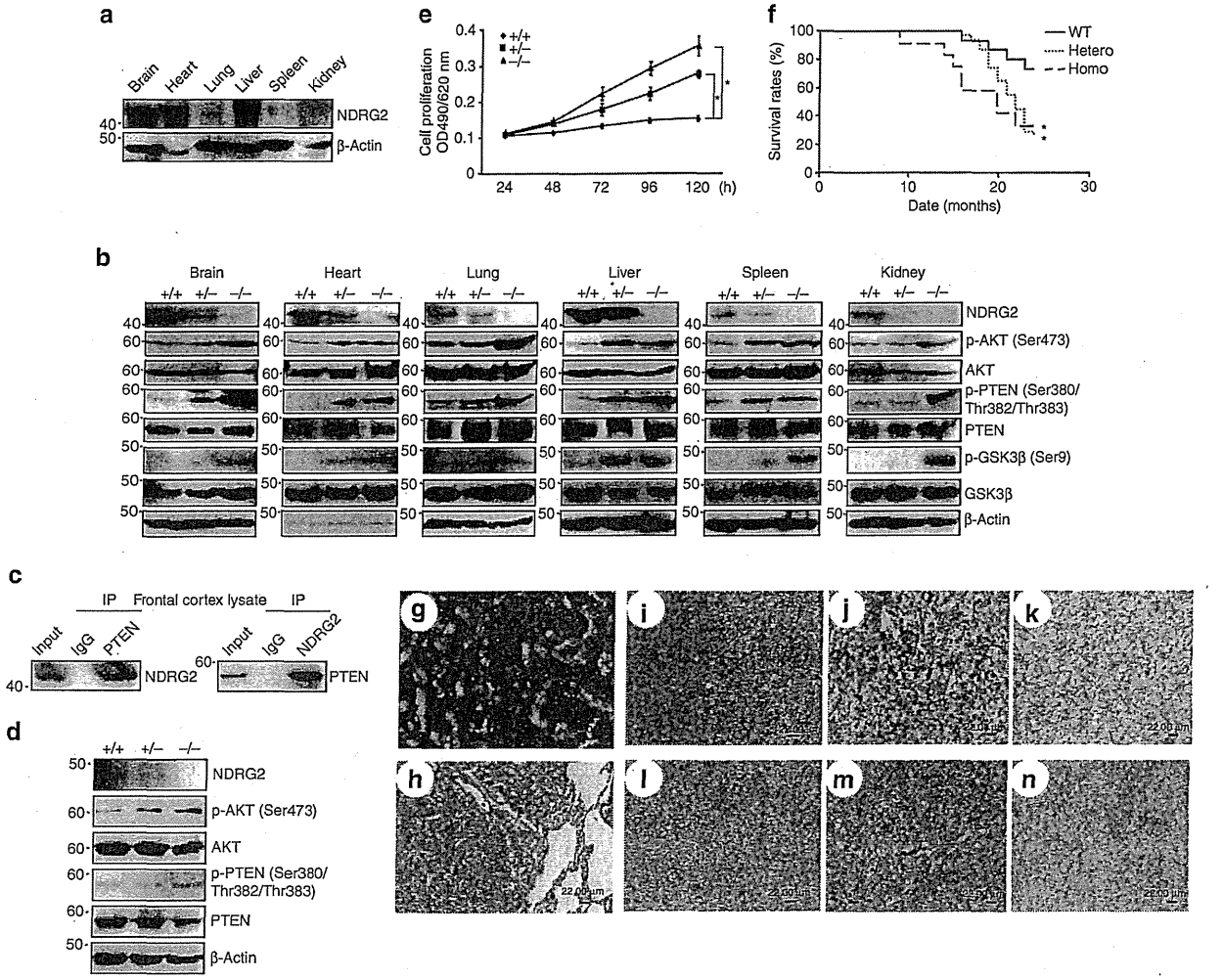

Figure 6 | *NDRG2*-deficient mice are susceptible to tumour formation. (**a**) Western blots of 3-month-old adult tissues of WT mice. The data are representative of two experiments. (**b**) Western blots of various tissues of 3-month-old *NDRG2*-deficient mice. The data are representative of two experiments. (**c**) The co-immunoprecipitation of PTEN and NDRG2 in frontal cortex homogenates from 3-month-old WT mice. The data are representative of three experiments. (**d**) Whole-cell lysates from WT, *NDRG2*$^{+/-}$ and *NDRG2*$^{-/-}$ embryonic fibroblasts were subjected to western blotting. (**e**) The proliferation rates of WT, *NDRG2*$^{+/-}$, and *NDRG2*$^{-/-}$ embryonic fibroblasts. The mean ± s.d. is shown; *$P<0.05$ (Student's *t*-test). The data are representative of three experiments. (**f**) Kaplan–Meier survival curves of WT ($n=15$), *NDRG2*$^{+/-}$ ($n=31$) and *NDRG2*$^{-/-}$ ($n=12$) mice up to 24 months of age. The difference in survival was statistically significant between WT and *NDRG2*$^{+/-}$ or *NDRG2*$^{-/-}$ mice (*$P<0.05$, log-rank test). (**g**) A hepatocellular carcinoma section from an *NDRG2*$^{+/-}$ mouse liver was subjected to H&E staining. The results indicated the presence of a large sheet of hepatic cords composed of several hepatocytes of variable nuclei and cell sizes; the nuclei of the carcinoma cells were hyperchromatic with prominent nucleoli (scale bar, 22 μm). (**h**) A bronchoalveolar carcinoma section from an *NDRG2*$^{+/-}$ mouse lung was subjected to H&E staining. The histopathology demonstrated a well-circumscribed mass of a solid sheet of neoplastic cells containing hyperchromatic nuclei with signs of frequent mitosis and an indistinct basophilic cytoplasm (scale bar, 22 μm). (**i–k**) Lymphoma sections from the mesenteric lymph node of an *NDRG2*$^{+/-}$ mouse. The histopathology indicated the presence of diffuse pleomorphic large lymphoid cells with vesicular nuclei, prominent nucleoli and scant cytoplasm (**i**). Robust staining for CD3 was present in the cytoplasm (**j**), but B220 staining was negative (**k**) (scale bar, 22 μm). (**l–n**) Lymphoma sections from an *NDRG2*$^{+/-}$ mouse spleen were examined by histopathology. The results demonstrated pleomorphic large lymphoid cells with vesicular nuclei, prominent nucleoli, some nuclear distortion and numerous cells undergoing mitosis (**l**). Staining for CD3 revealed robust cytoplasmic staining in cells, ranging from white pulp to red pulp (**m**). B220 staining was negative (**n**) (scale bar, 22 μm).

In accordance with previous studies[30,31], methylation of the *NDRG2* promoter was found in various cancer types (Supplementary Table 7; Fig. 7a). We confirmed that treatment of these cancer cell lines with 5-aza-deoxycytidine resulted in an increased abundance of *NDRG2* mRNA (Fig. 7b). Recently, we reported that the abundance of phosphorylated AKT-Ser473 inversely correlated well with NDRG2 protein abundance in the majority of oral squamous cell carcinoma (OSCC) cases[32], which are known to have very low frequencies of *PTEN* and *PIK3CA* mutations[33,34]. We found that cancer cell lines with low levels of NDRG2 show high levels of phosphorylated PTEN-Ser380/Thr382/Thr383 and AKT-Ser473 (Fig. 7c). Of note, we found that the ectopic expression of NDRG2 in two human cancer cell lines carrying WT *PTEN* ((SAS (OSCC) and HeLa (cervical cancer)) resulted in marked decreases in PTEN-Ser380/Thr382/Thr383 phosphorylation and PI3K-AKT inactivation (Fig. 7d). These findings suggest that down-regulation of *NDRG2* could have an important role in activating the PI3K-AKT signalling pathway in various types of cancer.